

Inertial particle trapping in an open vortical flow

Jean-Régis Angilella,¹ Rafael D. Vilela,² and Adilson E. Motter³

¹*Université de Caen et de Basse Normandie, LUSAC, Cherbourg, France*

²*Centro de Matemática, Computação e Cognição, Universidade Federal do ABC (UFABC),
Santo André-SP, 09210-170, Brazil*

³*Department of Physics and Astronomy, Northwestern University, Evanston, IL 60208, USA*

Abstract

Recent numerical results on advection dynamics have shown that particles denser than the fluid can remain trapped indefinitely in a bounded region of an open fluid flow. Here, we investigate this counterintuitive phenomenon both numerically and analytically to establish the conditions under which the underlying particle-trapping attractors can form. We focus on a two-dimensional open flow composed of a pair of vortices and its specular image, which is a system we represent as a vortex pair plus a wall along the symmetry line. Considering particles that are much denser than the fluid, referred to as *heavy particles*, we show that two attractors form in the neighborhood of the vortex pair provided that the particle Stokes number is smaller than a critical value of order unity. In the absence of the wall, the attractors are fixed points in the frame rotating with the vortex pair, and the boundaries of their basins of attraction are smooth. When the wall is present, the point attractors describe counter-rotating ellipses in this frame, with a period equal to half the period of one isolated vortex pair. The basin boundaries remain smooth if the distance from the vortex pair to the wall is large. However, these boundaries are shown to become fractal if the distance to the wall is smaller than a critical distance that scales with the inverse square root of the Stokes number. This transformation is related to the breakdown of a separatrix that gives rise to a heteroclinic tangle close to the vortices, which we describe using a Melnikov function. For an even smaller distance to the wall, we demonstrate that a second separatrix breaks down and a new heteroclinic tangle forms farther away from the vortices, at the boundary between the open and closed streamlines. Particles released in the *open* part of the flow can approach the attractors and be trapped permanently provided that they cross the two separatrices, which can occur under the effect of flow unsteadiness. Furthermore, the trapping of heavy particles from the open flow is shown to be robust to the presence of viscosity, noise, and gravity. Navier-Stokes simulations for large flow Reynolds numbers show that viscosity does not destroy the attracting points until vortex merging takes place, while simulation of thermal noise shows that particle trapping persists for extended periods provided that the Péclet number is large. The presence of a gravitational field does not alter the permanent trapping by the attracting points if the settling velocities are not too large. For larger settling velocities, however, gravity can also give rise to a limit-cycle attractor next to the external separatrix and to a new form of trapping from the open flow that is not mediated by a heteroclinic tangle.

I. INTRODUCTION

The motion of particles transported by a fluid flow can be very complex even when the particles are passive, the dynamics is non-brownian, and the flow is laminar [3–5, 13, 21, 26, 34, 35, 37]. Contributing to this complexity, the trajectories of particles with small but finite inertia often deviate significantly from fluid-point trajectories. The prediction of particle evolution is therefore a challenging task in particle-laden flows. In the paradigmatic case of spherical particles with small Reynolds numbers, the Maxey-Riley equation [25, 38] can be used to describe the particle dynamics provided that the fluid velocity field is known. For non-interacting particles, as considered in this study, the complexity of this dynamics is mainly due to the spatial and temporal dependencies of the fluid velocity, which are strongly nonlinear in general.

Previous theoretical analyses reported evidence of particle accumulation in well-defined regions of both laminar flows [35, 48, 50, 53, 57] and turbulent or random flows [6, 8, 20, 23, 24, 41, 55, 59, 60]. Particle clustering can occur even when the fluid itself is incompressible, and this is a property of major importance for the understanding of many natural and industrial advection processes [7, 15, 22, 33, 43, 47]. In bounded or periodic domains, this clustering behavior may be expected since particles have dissipative dynamics due to their inertia and dissipation can give rise to attractors. In *closed* vortical flows, such attractors tend to be associated with inward motion in the case particles less dense than the fluid—so-called bubbles—and with outward (but necessarily bounded) motion in the case of particles denser than the fluid [35]—also known as aerosols. Similar phenomenology is expected, and actually observed, for bubbles in *open* vortical flows [9, 10].

For aerosols, however, the possibility of permanent clustering of particles in open flows is far less clear. This is the case not only because particle motion is no longer constrained to be bounded but also because the same fluid velocity fields that have the potential to generate attractors tend to centrifuge denser particles away. Nevertheless, such attractor formation and consequent particle clustering has been shown to be possible for aerosols due to “interactions” between coexisting vortices [57]. This was demonstrated, for example, in numerical simulations of the open flow defined by leapfrogging vortices, where aerosols are trapped permanently by attracting points in the neighborhood of the vortices. The goal of the present paper is to determine both numerically *and* analytically the fluid and particle conditions under which such attracting sets exist, and investigate their properties as well as the properties of the associated basins of attraction.

Here, we consider small spherical particles much denser than the fluid, referred to as *heavy particles*, which capture the essential features of the problem while making it amenable to mathematical treatment. We focus on a system formed by two point-vortex pairs separated by a symmetry line, which is an open flow system that we represent as a single vortex pair plus a wall at the symmetry line (Fig. 1(a)). Accordingly, the flow Reynolds number is assumed to be much larger than one (inviscid fluid approximation), even though the particle Reynolds number, based on the slip velocity and on the particle diameter, will be assumed to be small throughout this paper. We concentrate on the limit

$$\varepsilon = \frac{d_0}{L_0} \ll 1, \tag{1}$$

where d_0 is the average half-distance between the vortices and L_0 is the distance from the

center of vorticity of the vortex pair to the wall (Fig. 1(b)). Due to the presence of the wall, the center of vorticity moves with respect to the distant fluid with velocity $v = \Gamma/(2\pi L_0)$ to first order in ε , where Γ is the strength of each vortex. In the small- ε regime, we can generalize analytical results on particle accumulation previously established for the closed-flow system defined by isolated (non-translating) point-vortex pairs with identical strengths [1]. Our analysis is partially based on using a perturbative fluid velocity field with respect to ε , where the case of an isolated vortex pair corresponds to $\varepsilon = 0$ (i.e., the absence of the wall) in our system.

In the reference frame translating with the center of vorticity, this flow exhibits open streamlines separated from closed streamlines by a separatrix formed by the invariant manifolds of two stagnation points (Fig. 2). A central part of this work concerns the demonstration that, under appropriate conditions, heavy particles from the open flow can approach the vortices and be captured by attracting points in their neighborhood. In addition to this external separatrix, which we denote Σ_3 , we anticipate that there are three other internal separatrices, denoted Σ_i for $i = 0, 1, 2$, which are located in the very neighborhood of the vortices and will be analyzed in the reference frame rotating with the vortex pair. These separatrices too will be shown to play a key role in the dynamics of inertial particles.

The motion of particles in this open vortical flow is investigated in Sec. II, where we show that attracting points exist even if $\varepsilon > 0$ provided that the particle Stokes number is small. In Sec. III, we show that the boundaries of the corresponding basins of attraction, which are smooth for $\varepsilon = 0$, become fractal if ε is above a critical value that decreases with increasing Stokes number. The occurrence of trapping from the open flow—for particles released far ahead of the vortex system in the upstream flow—is established and analyzed in Sec. IV. In Sec. V, we show that particle trapping is largely robust to the effects of gravity, viscosity, and noise. In the same section we also show that gravity can induce the formation of a new (limit-cycle) attractor, that potential flow theory provides a good approximation to predict heavy particle dynamics preceding vortex coalescence, and that noise can often enhance (rather than suppress) particle trapping. Final remarks are presented in Sec. VI. We use no-slip initial conditions in all simulations (i.e., the particles are released with velocity equal to the local fluid velocity), which corresponds to 2-dimensional slices of the basins of attraction and nevertheless reveals geometric properties of the full basins.

II. TRAPPING OF HEAVY PARTICLES NEAR VORTICES

For heavy particles, as considered here, it has recently been shown via analytical calculations that a system comprised of two co-rotating identical point vortices has two fixed-point attractors in the rotating frame for Stokes numbers smaller than $2 - \sqrt{3}$. This holds true when the vortex pair is isolated, forming a closed fluid flow system since in this case the center of vorticity does not translate with respect to the fluid [1]. The presence of a wall, on the other hand, allows the fluid to translate with respect to the vortex pair. This leads to a fundamentally different physical situation, in which the fluid flow system can now be open. In this section, by focusing on the velocity field in the neighborhood of the vortex pair, we study the persistency of the attractors and the properties of their attraction basins as a function of the Stokes number and distance of the vortices from the wall. In particular, we establish a relation between the emergence of fractal basin boundaries and the breakdown

of a separatrix in the neighborhood of the vortices.

A. Perturbative internal fluid velocity field

We first recall results of [2], where a perturbative expansion in ε was used to calculate the velocity field of the fluid for small ε , when the vortex pair (A, B) is distant from the wall. For $\varepsilon = 0$ (i.e., in the absence of the wall), the vortices rotate around their center point I with an angular velocity $\Omega_0 = \Gamma/(4\pi d_0^2)$, where the distance $2d_0 = |AB|$ between the vortices remains constant over time. We make use of Ω_0 and d_0 to set our equations non-dimensional in this section. The non-dimensional vortex strength is therefore equal to 4π . For $\varepsilon > 0$ (i.e., in the presence of the wall), the streamfunction is the sum of the flow induced by the two vortices plus the flow induced by the two mirror vortices, as illustrated in Fig. 2(a). Under the effect of the mirror vortices, the point I will translate in the x -direction with a non-dimensional velocity equal to $2\varepsilon + O(\varepsilon^3)$. In the neighborhood of (A, B) , the contribution from the mirror vortices is a perturbation taking the form of a straining flow. The resulting non-dimensional streamfunction in the reference frame $x''Iy''$ translating with I at velocity 2ε , reads

$$\psi_I(x'', y'', t) = \sum_{i=1}^2 -\ln [(x'' - x_i'')^2 + (y'' - y_i'')^2] + \frac{\varepsilon^2}{2}(x''^2 - y''^2) + O(\varepsilon^3), \quad (2)$$

where $(x_i''(t), y_i''(t))$ are the Cartesian coordinates of the vortices (A, B) . Because this streamfunction is valid near the vortices only, we refer to Eq. (2) as an *internal perturbative solution*. Figure 2(b) shows a comparison for $\varepsilon = 0.25$ between the exact potential flow induced by the four vortices and the perturbative solution. Even though ε is not very small, the streamlines are essentially undistinguishable in the neighborhood of the vortices. We have checked that the agreement is also satisfactory for the values of the velocity. Significant discrepancies start to appear at distances of about 3 non-dimensional units from I . In particular, the stagnation points S_1 and S_2 appearing on the symmetry line are not captured by the internal perturbative model, since they are points where the contribution of the two upper and two lower vortices have equal amplitudes and opposite signs.

One can verify that the dynamics of the vortices in this simplified flow satisfies $x_1''(t) = r(t) \cos \theta(t)$, $y_1''(t) = r(t) \sin \theta(t)$, $x_2'' = -x_1''$, and $y_2'' = -y_1''$, with $r(t) = 1 + (\varepsilon^2/2) \cos 2t$ and $\theta(t) = t - \varepsilon^2 \sin 2t$, plus terms of order ε^4 . The distance $2r(t)$ between the two vortices therefore oscillates with a period π (half the period of the isolated vortex pair, where throughout this paper we define the period as the time for each vortex to return to its original position in the coordinate system $x''Iy''$). In addition, the angular velocity of the vortices around I is affected by a perturbation with period π . This periodic forcing corresponds to the effect of a wall-induced straining flow on the vortices (see also [12] and [39] for vortex pairs in a straining flow).

It is well known that in the absence of the wall the velocity field is steady when observed in the rotating frame of the two vortices. It is therefore useful to re-write the streamfunction (2) in the coordinate system XIY defined on this rotating frame: $\psi_r(X, Y, t) = \psi_I(x'', y'', t) + (X^2 + Y^2)/2$. Assuming that the axes IX and IY correspond to Ix'' and Iy'' at $t = 0$, the

perturbative streamfunction reads

$$\psi_r(X, Y, t) = \psi_{r0}(X, Y) + \varepsilon^2 \psi_{r2}(X, Y, t), \quad (3)$$

where $Z = X + iY$, $\psi_{r0}(X, Y) = -2 \ln|Z^2 - 1| + |Z|^2/2$, and $\psi_{r2}(X, Y, t) = -\frac{2}{|Z^2 - 1|^2}[(Y^2 - X^2 + 1) \cos 2t + 4XY \sin 2t] + \frac{1}{2}[(X^2 - Y^2) \cos 2t - 2XY \sin 2t]$ [2]. The fluid velocity field in the rotating frame then takes the form

$$\mathbf{W}_f(X, Y, t) = \frac{\partial \psi_r}{\partial Y} \hat{\mathbf{X}} - \frac{\partial \psi_r}{\partial X} \hat{\mathbf{Y}} = \mathbf{W}_0(X, Y) + \varepsilon^2 \mathbf{W}_2(X, Y, t), \quad (4)$$

where $\mathbf{W}_2(X, Y, t) = \mathbf{W}_{2c}(X, Y) \cos 2t + \mathbf{W}_{2s}(X, Y) \sin 2t$, and the expressions of the steady fields \mathbf{W}_{2c} and \mathbf{W}_{2s} are obtained by differentiating with respect to the spatial variables the coefficients of $\cos 2t$ and $\sin 2t$ appearing in ψ_{r2} . In the next subsection, we investigate for the first time the motion of heavy particles in this flow.

B. Particle motion and attracting points

In the rotating reference frame, the equation of motion for such a heavy particle is [25, 38]

$$\frac{d^2 \mathbf{X}_p}{dt^2} = \frac{1}{St} \left(\mathbf{W}_f - \frac{d\mathbf{X}_p}{dt} \right) + \mathbf{X}_p - 2\hat{\mathbf{z}} \times \frac{d\mathbf{X}_p}{dt}, \quad (5)$$

where \mathbf{X}_p is the position vector of the particle, $St = \Omega_0 \tau_p$ is the Stokes number, τ_p is the particle relaxation time, and $\hat{\mathbf{z}}$ is the unit vector along the z -axis (perpendicular to the plane). The first term on the right side of this equation is the drag force, the second term is the centrifugal force, and the last term is the Coriolis force. In the rotating frame, the force due to the undisturbed flow also contains terms equal to the opposite of the Coriolis and centrifugal forces acting on the fluid. These forces, as well as the added mass, history, buoyancy, and lift forces [44], have not been taken into account since they are negligible for sufficiently small and heavy particles. The settling velocities are assumed to be negligible throughout the paper, except in Sec. V A, where the effect of gravity is considered in detail.

When $\varepsilon = 0$, there are four equilibrium positions (in addition to I) where the particle drag balances the centrifugal force if $St < 2 - \sqrt{3}$ or $St > 2 + \sqrt{3}$. Two of them are stable if $St < 2 - \sqrt{3}$, while the others are always unstable. The stable points, which we denote $\pm \mathbf{X}_{eq}$, are symmetric with respect to I ; their polar coordinates, defined by $\pm \mathbf{X}_{eq} \cdot \hat{\mathbf{X}} = R \cos \Theta$ and $\pm \mathbf{X}_{eq} \cdot \hat{\mathbf{Y}} = R \sin \Theta$, read

$$R = \sqrt{\cos 2\Theta + \frac{\sin 2\Theta}{St}}, \quad (6)$$

$$\Theta = \pm \frac{\pi}{2} \mp \frac{1}{2} \arcsin \frac{4St}{1 + St^2}. \quad (7)$$

These equilibrium points no longer exist when $\varepsilon > 0$, since the flow is no longer time-independent in the rotating frame XIY . Nevertheless, particles can be attracted to *moving* stable points in the vicinity of the equilibrium points $\pm \mathbf{X}_{eq}$ that exist for $\varepsilon = 0$ (they are in fact limit cycles in the extended phase space that includes time as one of the dimensions).

To analyze this effect, we employ the method used by [32] for particles in a periodic box. We focus on the vicinity of \mathbf{X}_{eq} , as the corresponding considerations for $-\mathbf{X}_{eq}$ follow immediately by symmetry. Replacing $\mathbf{X}_p(t) = \mathbf{X}_{eq} + \mathbf{h}(t)$ in the equation of motion (5) and performing a Taylor expansion with respect to $\mathbf{h}(t)$, we obtain

$$\frac{d^2\mathbf{h}}{dt^2} = \frac{1}{\text{St}} \left[\mathbf{h} \cdot \nabla \mathbf{W}_{0,eq} + \varepsilon^2 (\mathbf{W}_{2c}(\mathbf{X}_{eq}) \cos 2t + \mathbf{W}_{2s}(\mathbf{X}_{eq}) \sin 2t) - \frac{d\mathbf{h}}{dt} \right] + \mathbf{h} - 2\hat{\mathbf{z}} \times \frac{d\mathbf{h}}{dt}, \quad (8)$$

where $\nabla \mathbf{W}_{0,eq}$ is the gradient tensor of the fluid velocity \mathbf{W}_0 at \mathbf{X}_{eq} . In this expression, terms of order $|\mathbf{h}|^2$ and $\varepsilon^2|\mathbf{h}|$ have been neglected. The solution of this linear non-homogeneous equation is the sum of a particular solution $\mathbf{h}_a(t)$ of the full equation and the general solution $\mathbf{h}_b(t)$ of the homogeneous part of the equation.

By setting $\mathbf{h}_a(t) = \mathbf{p} \cos 2t + \mathbf{q} \sin 2t$ in Eq. (8), we are led to the following conditions for the coefficients of $\cos 2t$ and $\sin 2t$ [32]:

$$\mathbf{L}\mathbf{p} - \mathbf{M}\mathbf{q} = -\frac{\varepsilon^2}{\text{St}} \mathbf{W}_{2c}(\mathbf{X}_{eq}), \quad (9)$$

$$\mathbf{L}\mathbf{q} + \mathbf{M}\mathbf{p} = -\frac{\varepsilon^2}{\text{St}} \mathbf{W}_{2s}(\mathbf{X}_{eq}), \quad (10)$$

with

$$\mathbf{L} = \frac{1}{\text{St}} \nabla \mathbf{W}_{0,eq} + 5\mathbf{I} \quad (11)$$

and

$$\mathbf{M} = \frac{2}{\text{St}} \mathbf{I} + 4\mathbf{A}, \quad (12)$$

where $\mathbf{A} = \begin{pmatrix} 0 & -1 \\ 1 & 0 \end{pmatrix}$ and \mathbf{I} is the identity matrix. One can easily check that \mathbf{M} and \mathbf{L} are invertible, where the latter follows from the eigenvalues of the attracting points having strictly nonzero real parts (and hence $\nabla \mathbf{W}_{0,eq}$ being non-singular). It follows that

$$(\mathbf{M}^{-1}\mathbf{L} + \mathbf{L}^{-1}\mathbf{M}) \mathbf{q} = \frac{\varepsilon^2}{\text{St}} (\mathbf{L}^{-1}\mathbf{W}_{2c}(\mathbf{X}_{eq}) - \mathbf{M}^{-1}\mathbf{W}_{2s}(\mathbf{X}_{eq})), \quad (13)$$

$$(\mathbf{M}^{-1}\mathbf{L} + \mathbf{L}^{-1}\mathbf{M}) \mathbf{p} = -\frac{\varepsilon^2}{\text{St}} (\mathbf{L}^{-1}\mathbf{W}_{2s}(\mathbf{X}_{eq}) + \mathbf{M}^{-1}\mathbf{W}_{2c}(\mathbf{X}_{eq})). \quad (14)$$

By solving this system, one can obtain a closed form for \mathbf{p} and \mathbf{q} , and this provides a particular solution to Eq. (8). An approximate expression can be found for $\text{St} \ll 1$ by performing a Taylor expansion of both \mathbf{X}_{eq} and the various matrices in terms of St . To first order in St , the solution reads

$$\mathbf{h}_a(t) = \sqrt{3}\varepsilon^2 \left(\frac{2124}{169} \text{St} \cos 2t - \frac{15}{13} \sin 2t \right) \hat{\mathbf{X}} - \sqrt{3}\varepsilon^2 \left(\frac{27}{26} \cos 2t + \frac{752}{169} \text{St} \sin 2t \right) \hat{\mathbf{Y}}. \quad (15)$$

This solution corresponds to particles on an elliptic trajectory rotating with period π in the clockwise direction around \mathbf{X}_{eq} in the rotating frame.

The general solution $\mathbf{h}_b(t)$ of the homogeneous part of Eq. (8) is nothing more than a perturbation around \mathbf{X}_{eq} for $\varepsilon = 0$. Because the corresponding eigenvalues have strictly

negative real parts for $St < 2 - \sqrt{3}$ [1], we infer that $\mathbf{h}_b(t) \rightarrow 0$ as $t \rightarrow \infty$. We thus conclude that particles are attracted to the vicinity of the points $\pm \mathbf{X}_{eq} + \mathbf{h}_a(t)$, where $\mathbf{h}_a(t)$ is the particular periodic solution approximated by Eq. (15). Note that, for capturing the effect of the wall, the solution $\mathbf{h}_a(t)$ cannot be anticipated from the existing literature on isolated vortex pairs.

Figure 3 shows a simulation of a particle cloud for $\varepsilon = 0.33$ and $St = 0.1$. Initially, the particles are distributed uniformly in the square $[-3, 3] \times [-3, 3]$, which includes the vortex pair, and have velocity equal to the local fluid velocity. The particle cloud is shown after 14 periods at four different instants (blue dots). We indeed observe that particles are attracted by two moving points rotating clockwise around $\pm \mathbf{X}_{eq}$ with a trajectory that is close to the elliptic orbit predicted theoretically in Eq. (15). The parameter ε has been taken rather large here to facilitate visualization, and agreement with the theoretical predictions only improves for smaller ε .

C. Crossing of the internal separatrix

We now turn to the emergence of chaos in the particle dynamics due to the perturbation of homoclinic and/or heteroclinic orbits. An homoclinic orbit in which branches of the stable and unstable manifolds of a fixed point (or, more generally, of a periodic orbit) coincide is a common structure in nonchaotic systems; the heteroclinic counterpart corresponds to the situation in which a branch of the stable manifold of one orbit coincides with a branch of the unstable manifold of another orbit. Generic perturbations of such systems typically lead such branches to no longer coincide. If the manifolds associated with the perturbed homoclinic (heteroclinic) orbit(s) are found to intersect transversely at one point, then they will intersect transversely at infinitely many points, forming a homoclinic (heteroclinic) tangle and, in particular, giving rise to a chaotic set around the original manifold. These transverse intersections can be detected using the Melnikov method, where such intersections correspond to isolated odd zeros of an integral function—the Melnikov function—which provides a measure of the signed distance between the stable and unstable manifolds [29, 46].

In order to proceed with our analysis of the particle dynamics in the internal perturbative flow, we first compare the order of magnitude of the various forces appearing in the equation of motion (5) with the approximate velocity field (4). Equation (5) contains two small parameters, namely St (accounting for inertia effects) and ε (accounting for the wall effect). Clearly, if $St \ll \varepsilon^2$, the velocity of the particle is only slightly modified by inertia. In contrast, if $St \gg \varepsilon^2$, particles do not feel the effect of the wall, as the corresponding oscillation of the vortices is weak. Therefore, we assume throughout that $St = O(\varepsilon^2)$ and set

$$St = k \varepsilon^2, \quad (16)$$

where k is a constant of order one. This condition is necessary to keep both the effect of the wall and the effect of inertia significant. Then, taking a perturbative solution of the equation of motion in the form [30, 31, 36]

$$\frac{d\mathbf{X}_p}{dt} = \mathbf{W}_f(\mathbf{X}_p, t) + St [\mathbf{X}_p - 2\hat{\mathbf{z}} \times \mathbf{W}_f(\mathbf{X}_p, t) - \mathbf{W}_f(\mathbf{X}_p, t) \cdot \nabla \mathbf{W}_f(\mathbf{X}_p, t)] + O(St^2), \quad (17)$$

we obtain

$$\frac{d\mathbf{X}_p}{dt} = \mathbf{W}_0(\mathbf{X}_p) + \varepsilon^2 \mathbf{W}_2(\mathbf{X}_p, t) + k\varepsilon^2 [\mathbf{X}_p - 2\hat{\mathbf{z}} \times \mathbf{W}_0(\mathbf{X}_p) - \mathbf{W}_0(\mathbf{X}_p) \cdot \nabla \mathbf{W}_0(\mathbf{X}_p)] + O(\varepsilon^4). \quad (18)$$

Under the given conditions, the dynamics of inertial particles is therefore equivalent to a Hamiltonian system perturbed by terms of order ε^2 . The unperturbed phase portrait is the same as the one of fluid particles, which is the well-known streamline diagram of co-rotating point-vortex pairs shown in Fig. 3. As indicated in that figure, this flow has two heteroclinic orbits, Σ_1 and Σ_2 , forming separatrices associated with the fixed points H and H' and has two homoclinic orbits, Σ_0 , which form separatrices associated with the fixed point I . The possibility of homoclinic and heteroclinic tangles in the internal perturbative flow can then be analyzed using the Melnikov method applied to these orbits.

Specifically, the Melnikov functions of the separatrices Σ_i for $i = 0, 1, 2$ will indicate whether, under the effect of the ε^2 perturbations, the invariant manifolds associated with the various hyperbolic points will intersect transversely or not. Transverse intersections imply that a chaotic set exists in the vicinity of Σ_i and that particles may experience transient chaotic behavior in this region before converging to one of the attracting points or being centrifuged away (although this is not necessarily the case in general, our numerics do not indicate any other outcome for the flow and parameters considered here). To first order in ε^2 , the transverse signed distance between the invariant manifolds associated with the separatrix Σ_i at some point $\mathbf{X}^* \in \Sigma_i$ is given by $d_i(t_0) = \varepsilon^2 a_i M_i(t_0)$, where a_i is independent of ε and M_i is the Melnikov function. For the separatrix Σ_i , we obtain

$$M_i(t_0) = \int_{-\infty}^{\infty} \dot{\mathbf{q}}_i(t) \times [\mathbf{W}_{2c}(\mathbf{q}_i(t)) \cos 2(t + t_0) + \mathbf{W}_{2s}(\mathbf{q}_i(t)) \sin 2(t + t_0)] dt + k \int_{-\infty}^{\infty} \dot{\mathbf{q}}_i(t) \times [\mathbf{q}_i(t) - 2\hat{\mathbf{z}} \times \dot{\mathbf{q}}_i(t) - \ddot{\mathbf{q}}_i(t)] dt, \quad (19)$$

where t_0 is the starting time of the stroboscopic map $\mathbf{X}_p(t) \rightarrow \mathbf{X}_p(t + \pi)$, and $\mathbf{q}_i(t)$ is a solution of the unperturbed system with $\mathbf{q}_i(0) = \mathbf{X}^*$. As t_0 varies, the manifolds evolve and any intersection between them will be detected at \mathbf{X}^* . Because $\mathbf{q}_i(t)$ does not depend on ε or St , we compute this solution numerically for $i = 0, 1, 2$ and use this solution to calculate the above integrals. Also, we make use of the fact that $\mathbf{q}_i(t)$ and its derivative are symmetric functions, so that some of the integrals vanish. This leads to

$$M_i(t_0) = \alpha_i \sin 2t_0 + k m_i, \quad (20)$$

where α_i and m_i are purely numerical constants. The former constants have been calculated in a previous work [2]: $\alpha_0 \approx -0.58$, $\alpha_1 \approx -0.89$, and $\alpha_2 \approx 7.3$. The latter constants are $m_0 \approx -42.1$, $m_1 \approx -25.8$, and $m_2 \approx 8.3$. Therefore, for any St or ε larger than zero, the Melnikov function is no longer zero for each of the three separatrices, indicating that the stable and unstable manifolds no longer coincide. The pertinent question is then whether they intersect each other transversely.

The α_i constants reflect the influence of the time dependence of the fluid flow on the splitting of the separatrices. The m_i 's account for the effect of the particles' inertia only. Function $M_i(t_0)$ has no zeros if $k > \max_{i=0,1,2} |\alpha_i|/|m_i| = |\alpha_2|/|m_2|$. This is equivalent to the condition

$$\text{St} > \text{St}_{c_2} \equiv \frac{|\alpha_2|}{|m_2|} \varepsilon^2, \quad (21)$$

where $|\alpha_2|/|m_2| \approx 0.88$. If this condition is fulfilled, the stable and unstable manifolds associated with the hyperbolic points I , H and H' of the stroboscopic map, which persist if ε is small enough, split apart but do not intersect each other: particles injected near the separatrices will evolve non-chaotically and eventually move either toward an attracting point or toward infinity. Conversely, if the inverse inequality is satisfied in Eq. (21), then it follows from Eq. (20) that $M_2(t_0)$ will have isolated odd zeros as a function of t_0 , and this implies the existence of a heteroclinic tangle. It is the separatrix Σ_2 that is represented in Eq. (21) because this separatrix is more sensitive than Σ_0 and Σ_1 to the presence of the wall: for a given Stokes number, if one increases ε so that $\text{St} < \text{St}_{c_2}$, the invariant manifolds of the separatrix Σ_2 will be the first to intersect transversely. If ε is further increased, i.e., if the distance from the wall is further reduced, then Σ_1 and Σ_0 will, in this order, give rise to chaotic sets by a similar mechanism.

Figure 4 summarizes these different behaviors. It shows the stable manifold W^s and unstable manifold W^u coinciding in the absence of both particle inertia and wall (Fig. 4(a)), split apart when particle inertia dominates (Fig. 4(b)), and intersecting each other transversely when the effect of the wall dominates (Fig. 4(c)). Very remarkably, particles outside the separatrix Σ_2 cannot reach the neighborhood of the attracting point \mathbf{X}_{eq} when the invariant manifolds are split apart. This is the case because, as indicated in Fig. 4(b), the velocity field of particle dynamics points outward in the region between W^s and W^u . That is, the stable manifold is encircled by the unstable one, which corresponds to positive values for the Melnikov function M_2 (according to the convention for the signed distance adopted in this paper). In this process, W^s can be regarded as a barrier to the transport of particles from the outside. However, it becomes possible for outside particles to reach the inner region (interior to $\Sigma_1 \cup \Sigma_2$) when the effect of the wall is dominant and induces transverse intersections between W^s and W^u . Indeed, in this case, certain particles located outside the stable manifold—those in the lobes limited by W^u [49]—are transported to the other side of the stable manifold after one period of the stroboscopic map. This tangle, and hence the transient chaos that comes with it, is a necessary (albeit not sufficient) condition for outside particles to eventually approach the attracting point.

Finally, because the Melnikov functions M_1 and M_0 are negative for St/ε^2 larger than $|\alpha_1|/|m_1|$ and $|\alpha_0|/|m_0|$, respectively, the reciprocal argument applies to the separatrices Σ_1 and Σ_0 . That is, the orientation of the particle-velocity field is such that these separatrices become permeable toward the interior of the $\Sigma_1 \cup \Sigma_2$ cycle as soon as their stable and unstable manifolds split apart (in contrast with Σ_2 , which requires the emergence of chaos, and hence larger ε , to become permeable). Physically, this occurs due to the centrifugation of the particles in the vicinity of the vortices.

These results can be interpreted also in terms of the distance between the vortices and the wall. Chaos exists in the vicinity of the vortices if and only if the vortex pair is placed below a critical distance $L_c \sim d_0/\sqrt{\text{St}}$ from the wall. Above this critical distance, the influence of the wall, and consequent oscillation in the inter-vortex separation, is too weak to induce chaos in the dynamics of inertial particles. On the other hand, since this critical distance scales as $\text{St}^{-1/2}$, for any large but finite distance between the vortex pair and the wall, chaos will always manifest itself for sufficiently small heavy particles. As shown in the next section, the existence of a chaotic set critically impacts the geometry of the basin boundaries of the attracting points.

III. FRACTAL BASIN BOUNDARIES

The appearance of a chaotic set in the vicinity of separatrices can drastically change the boundaries of the basins of attraction, since inertial particles can move erratically in that region before either approaching an attracting point or being centrifuged away. This transiently chaotic dynamics imprints a signature in the geometry of the boundaries between the different basins of attraction. We thus expect that the boundaries of the attraction basins will be smooth when no chaotic sets are present around the separatrices but become fractal when such sets exist and are sufficiently wide to be connected with the attraction basins.

We have verified this by computing the basins of attraction numerically. Specifically, we plotted the initial (X, Y) conditions of the trapped particles color-coded according to which of the two attractors they approach asymptotically. Typical attraction basins computed through this procedure are shown in Fig. 5 for $St = 0.02$ and in Fig. 6 for $St = 0.07$; these figures were generated using 2×10^5 particles initially uniformly distributed in a square region covering the vortices and released with initial velocity equal to the local fluid velocity. For $St = 0.02$, Eq. (21) predicts the formation of a heteroclinic tangle at $\varepsilon \approx 0.15$. Indeed, Fig. 5 shows that the basin boundaries appear smooth for $\varepsilon = 0.1$ but have filamentary characteristics for $\varepsilon = 0.2$. In order to check the predictions of the perturbative model in Eq. (4), we have also computed the same attraction basins for particles advected by the exact four-vortex potential flow. Even though the detailed structure of the filaments is different, the overall shape of the basins obtained from the perturbative flow is close to the one obtained from the exact velocity field even for relatively large ε (Figs. 5(b) and 5(e), respectively). Similarly, for $St = 0.07$ the theory predicts the formation of a heteroclinic tangle at $\varepsilon \approx 0.28$, in agreement with the basins shown in Fig. 6. As expected, for larger ε 's—as used in Figs. 6(b) and 6(e)—more significant discrepancies appear between the perturbative and exact flow simulations. In particular, the external heteroclinic orbit Σ_3 (considered in the next section) is closer to the vortices and may affect the particle dynamics, and this effect is not captured by the internal perturbative model.

In order to further validate the predictive power of Eq. (21) we have computed the fractal dimension of the basin boundaries for various ε 's and various Stokes numbers. The dimension can be computed efficiently and accurately from a sample of representative points in the boundary [28]. To generate a set of such points we applied bisection on a segment of line cutting the basin boundary. Specifically, to search for a point in the boundary we randomly pick a pair of points in the line segment $x = 2.3$ and $-1 \leq y \leq 1$, which is close to Σ_2 , the first separatrix to break as the perturbation parameter ε increases. The pair is discarded if both points are found to be in the same basin of attraction. Otherwise we determine the basin to which the midpoint of the segment joining that pair belongs. This allows us to form a pair of points closer to each other belonging to different basins. The procedure is repeated until we obtain points belonging to different basins and at a distance from each other that does not exceed some pre-defined threshold $2d_{thr}$. This implies that the midpoint of the final pair is less than d_{thr} -apart from the basin boundary and hence serves as a good approximation to a point in the boundary. After identifying a few hundred such points using this algorithm, we applied a method introduced in [28] to compute the dimension. The method is based on the scaling $\langle 1/N_i(R) \rangle \sim R^{-D^{(1)}}$, where $N_i(R)$ is the number of sampled points within a ball of radius R centered at the i -th point and $\langle \cdot \rangle$ denotes the average over all i . The dimension $D^{(1)}$ refers to the intersection set between

the basin boundary and the initial line segment, while the dimension of the basin boundary in 2-dimensional portraits such as those in Figs. 5 and 6 is simply $D^{(2)} = 1 + D^{(1)}$. The dimension of the basin boundary in the full 4-dimensional phase space of the inertial particle dynamics is $D^{(4)} = 3 + D^{(1)}$.

Figure 7 shows $D^{(2)}$ versus St for $\varepsilon = 0.2$. In this case, Eq. (21) predicts that a heteroclinic tangle exists when $St < 0.88 \varepsilon^2 \approx 0.035$. We indeed observe that the basin boundary is fractal ($D^{(2)} > 1$) when $St \lesssim 0.035$ and smooth ($D^{(2)} = 1$) otherwise. Figure 8 shows $D^{(2)}$ versus ε for $St = 0.03$. In this case, Eq. (21) predicts that a heteroclinic tangle exists when $\varepsilon > (St/0.88)^{1/2} \approx 0.185$. This corresponds to the critical distance to the wall below which the particle dynamics becomes chaotic in the vicinity of the separatrix Σ_2 . The numerical calculation shown in Fig. 8 confirms that the basin boundary is indeed smooth for $\varepsilon \lesssim 0.185$ and fractal for larger ε . This is consistent with the expectation that the chaotic set around this (internal) separatrix gives rise to the fractal structure of the basin boundary.

Next, we consider the flow further away from the attractors and the (external) separatrix that exists between bounded and unbounded streamlines.

IV. TRAPPING OF HEAVY PARTICLES FROM THE OPEN FLOW

The flow investigated in the previous sections is bounded by the heteroclinic orbit Σ_3 (Fig. 2(a), bold curve). This external separatrix is the boundary between the closed streamlines near the vortices and the open streamlines going to infinity. When the Stokes number is sufficiently small, the velocity of the particles is close to the local fluid velocity and hence the separatrix Σ_3 also appears in the leading-order phase portrait of inertial particles. Yet, for any nonzero inertia, the corresponding invariant manifolds associated with the saddle points S_1 and S_2 no longer coincide. Nevertheless, as we show below, no particles from outside can cross the separatrix if the invariant manifolds split apart. This is so because the invariant manifolds shield the flow region internal to Σ_3 through a mechanism analogous to the one described in Fig. 4 for the separatrix Σ_2 . Under these circumstances, particles released outside Σ_3 will never reach the neighborhood of the vortices and will never be captured by the attractors investigated in Sec. II. The scenarios in which the trapping of particles from the open flow occurs are investigated in this section. We show that, as in the case of the separatrix Σ_2 , the emergence of transverse intersections between the invariant manifolds is a necessary condition for particles to cross the separatrix Σ_3 .

A. Perturbative external fluid velocity field

The typical length and velocity scales of the flow near the separatrix Σ_3 are L_0 and Γ/L_0 , respectively. Hence, we non-dimensionalize the streamfunction by using L_0 for lengths and $\Gamma/4\pi L_0$ for velocities. This non-dimensionalization is different from the one introduced in Sec. II for the internal flow. In the analyses below we continue to use the same notation for the dynamical variables with respect to the new non-dimensionalization. To facilitate comparisons, however, in all figures we continue to use spatial coordinates normalized by d_0 , as done in our analysis of the internal flow.

From the external separatrix, to first approximation, each pair of vortices can be seen as a single vortex. Therefore, we make use of the reference frame $x'O'y'$ translating with respect to the laboratory frame xOy at velocity v_0 , which is the leading order of the velocity of the vortex pair. In this translating frame, the non-dimensional streamfunction of the flow induced by the vortex pair plus its mirror is $\psi_E(x', y') = (\psi - v_0 y')/\Gamma/4\pi$, where $\psi(x, y, t)$ is the streamfunction of the flow observed in the laboratory frame. Still assuming that $\varepsilon = d_0/L_0 \ll 1$, the streamfunction can be expanded as [2]

$$\psi_E(x', y') = \psi_0(x', y') + \varepsilon^2 \psi_c(x', y') \cos \frac{2t}{\varepsilon^2} + \varepsilon^2 \psi_s(x', y') \sin \frac{2t}{\varepsilon^2} + O(\varepsilon^4), \quad (22)$$

where $\psi_0(x', y')$ is the streamfunction of a simple dipole centered at (0,0) (i.e., a single vortex plus its mirror vortex) and the ε^2 terms express the fact that in reality we have vortex *pairs* and the resulting flow is unsteady.

B. Crossing of the external separatrix

The characteristic time of the flow close to the external separatrix is ε^{-2} times larger than the characteristic time of the flow close to the internal separatrices. The Stokes number for heavy particle dynamics near Σ_3 is therefore equal to $\varepsilon^2 \text{St}$, where St is the previously introduced particle Stokes number in the internal flow. The equation of motion of the particles in the velocity field corresponding to the streamfunction (22) then reads (removing the star superscripts for clarity and neglecting terms of order higher than two in the fluid velocity),

$$\frac{d^2 \mathbf{X}_p}{dt^2} = \frac{1}{\varepsilon^2 \text{St}} \left(\mathbf{V}_0(\mathbf{X}_p) + \varepsilon^2 \mathbf{V}_{2c}(\mathbf{X}_p) \cos \frac{2t}{\varepsilon^2} + \varepsilon^2 \mathbf{V}_{2s}(\mathbf{X}_p) \sin \frac{2t}{\varepsilon^2} - \frac{d\mathbf{X}_p}{dt} \right), \quad (23)$$

where the velocity fields \mathbf{V}_0 , \mathbf{V}_{2c} and \mathbf{V}_{2s} correspond to the streamfunctions ψ_0 , ψ_c and ψ_s respectively. Keeping St fixed and expanding the particle velocity in powers of ε , we obtain

$$\begin{aligned} \frac{d\mathbf{X}_p}{dt} = & \mathbf{V}_0 - \text{St} \varepsilon^2 \mathbf{V}_0 \cdot \nabla \mathbf{V}_0 + \varepsilon^2 (\mathbf{V}_{2c} - 2\text{St} \mathbf{V}_{2s}) \cos \frac{2t}{\varepsilon^2} \\ & + \varepsilon^2 (2\text{St} \mathbf{V}_{2c} + \mathbf{V}_{2s}) \sin \frac{2t}{\varepsilon^2} + O(\varepsilon^4, \varepsilon^2 \text{St}^2). \end{aligned} \quad (24)$$

We therefore have a rapidly perturbed Hamiltonian system, with a perturbation frequency $\sim \varepsilon^{-2}$ [27].

One can always calculate the Melnikov function $M(t_0)$ representing the signed distance between the unstable and stable manifolds of the saddle points S_1 and S_2 , respectively. But in this rapidly perturbed system the Melnikov function itself depends on ε , which contrasts with the Melnikov functions of the internal separatrices. Indeed, we obtain that

$$M(t_0) = -m \text{St} + A(\varepsilon) \left(\sin \frac{2t_0}{\varepsilon^2} - 2\text{St} \cos \frac{2t_0}{\varepsilon^2} \right), \quad (25)$$

where the constant m represents centrifuge effects and the amplitude $A(\varepsilon)$ is the contribution of the unsteady perturbation due to the rotation of the vortices around each other. To

the best of our knowledge, it has not been rigorously demonstrated that simple zeros in a Melnikov function of this form will necessarily imply that the dynamics is chaotic [27]. Nevertheless, the existence of such simple zeros of $M(t_0)$ guarantees that particles can cross Σ_3 in both directions, and hence that a fraction of particles from the open flow can enter the closed component of the flow. In contrast, a negative sign for all t_0 in the Melnikov function indicates that particles released outside cannot enter.

The constant m can be written as

$$m = \int_{-\infty}^{\infty} [\mathbf{V}_0 \times (\mathbf{V}_0 \cdot \nabla \mathbf{V}_0)](\mathbf{q}(t)) dt, \quad (26)$$

where $\mathbf{q}(t)$ is a solution of the unperturbed system on the separatrix Σ_3 , which we calculated numerically, leading to $m \simeq 30.4$. The amplitude of the oscillating part reads

$$A(\varepsilon) = \int_{-\infty}^{\infty} [\mathbf{V}_0 \times \mathbf{V}_{2s}](\mathbf{q}(t)) \cos \frac{2t}{\varepsilon^2} dt - \int_{-\infty}^{\infty} [\mathbf{V}_0 \times \mathbf{V}_{2c}](\mathbf{q}(t)) \sin \frac{2t}{\varepsilon^2} dt, \quad (27)$$

and was computed numerically using a grid for $\varepsilon \in [0, 0.5]$. The result was then fitted with a combination of exponential and rational functions of ε as

$$A(\varepsilon) \simeq \frac{e^{-\beta_3/\varepsilon^2}}{\varepsilon^2} (\beta_0 + \beta_2 \varepsilon^2), \quad (28)$$

where $\beta_0 \simeq 23.6$, $\beta_2 \simeq 46.0$, and $\beta_3 \simeq 0.63$. Finally, by imposing that the oscillatory part be smaller than the constant part of $M(t_0)$, we obtain a sufficient condition for Σ_3 to be closed for particles released outside:

$$\text{St} > \text{St}_{c_3}(\varepsilon) \equiv \frac{e^{-0.63/\varepsilon^2}}{\varepsilon^2} (0.78 - 1.51\varepsilon^2), \quad (29)$$

where the constants were replaced by their numerical values, and we made use of the fact that $|\sin(x) - 2\text{St} \cos(x)| \leq (1 + 4\text{St}^2)^{1/2}$ for all x . In addition, to obtain a simpler criterion, we have assumed that St^2 is small compared to 1. Because integrals have been fitted, Eq. (29) is a partially numerical criterion rather than a purely analytical one. Nevertheless, this formula is very useful to predict trapping from the open flow, and is used in the next section to construct the complete trapping diagram of particle dynamics in the vortical flow.

C. Trapping diagram

Figure 9 shows in the (ε, St) plane both the critical Stokes number St_{c_3} for the breakdown of the external separatrix Σ_3 (defined by the converse of Eq. (29)) and the critical Stokes number St_{c_2} for the breakdown of the internal separatrix Σ_2 (defined by the converse of Eq. (21)). Above curve $\text{St}_{c_2}(\varepsilon)$ the separatrix Σ_2 is “closed” (i.e., the stable and unstable manifolds do not intersect transversally, and cannot be crossed from the outside) and below this curve the separatrix Σ_2 is “open” (i.e., the manifolds intersect transversely and a chaotic set is formed near the separatrix). A similar characterization applies to the curve $\text{St}_{c_3}(\varepsilon)$ with respect to the separatrix Σ_3 . Because $\text{St}_{c_2} > \text{St}_{c_3}$ for $\varepsilon > 0$, the opening of Σ_3 implies that Σ_2 is also open. This does not mean that particles released outside and crossing Σ_3

will necessarily cross Σ_2 , since the tangles around each separatrix do not necessarily overlap. However, if trapping occurs for particles released outside Σ_3 , then the parameters must be in the region defined by $St < St_{c_3}(\varepsilon)$. That is, being in this region, and hence having both separatrices open, is a *necessary* condition for particle trapping from the open flow.

In order to check the theoretically-predicted trapping diagram, we have implemented numerical simulations using the exact four-vortex potential velocity field \mathbf{V}_f for the fluid and the dynamical equation of the particles in the laboratory frame (that is, Eq. (5) for \mathbf{W}_f replaced by \mathbf{V}_f and without the centrifugal and Coriolis forces). For given values of ε and St , we considered particles released far ahead of the vortices, outside Σ_3 and near the wall. They are driven by the flow toward the vicinity of S_1 and then around the vortex pair near Σ_3 , independently of the detailed shape of the initial distribution of particles. Trajectories were computed for a large number of turnover times, and the number $N(St)$ of particles crossing inside Σ_3 during this period of time was then counted. The critical Stokes number was estimated numerically in these simulations using a bisection procedure applied to $N(St)$, with the process terminated when the difference in St for crossing or not crossing the separatrix fell below a certain threshold. The result is plotted in Fig. 9 (circles): no particle released in the open flow is observed to cross Σ_3 when St is below the circles. We note that this numerical curve agrees with the theoretical value of St_{c_3} in Eq. (29) up to $\varepsilon \simeq 0.4$. For larger ε , that is when vortices are closer to the wall, the perturbative theory underestimates the critical Stokes number. This might be due to the fact that the wall-induced perturbation is underestimated by the perturbative velocity field there.

To further examine the validity of the trapping diagram, two simulations—corresponding to the parameters P_1 ($\varepsilon = 0.4, St = 0.09$) and P_2 ($\varepsilon = 0.4, St = 0.04$) in the diagram of Fig. 9—have been carried out for the exact potential velocity field induced by the four vortices. The initial positions of the vortices are $(\pm 1, \pm 1/\varepsilon)$, and particles are released in the rectangle $[-5, 10] \times [0, 5]$, extending to the open portion of the flow ahead of the vortices and meant to detect whether the attraction basins reach outside Σ_3 . The basins of attraction defined by these initial conditions are shown in Fig. 10. The basins of attraction extend outside the separatrix Σ_3 in the case of P_2 , and are contained within it in the case of P_1 . This is in accordance with our theoretical predictions that trapping from the open flow would be possible for P_2 but not for P_1 , which is also confirmed by direct simulations of both the perturbative and the exact potential velocity field. In the case of P_2 , this means that a fraction of the particles crossing Σ_3 can also cross Σ_2 and approach the attractors. We deduce that this mechanism underlies the trapping of heavy particles in the leapfrogging open vortical flow observed in the previous numerical study of [57]. Figure 10 also suggests that the probability of getting trapped from the outside is small, since the measure of the external portion of the basins is small compared to the volume of the tested region. However, the figure also indicates that this probability is much larger for particles released near the wall.

V. ROBUSTNESS OF TRAPPING

In the previous sections we have shown that our perturbative analysis successfully describes trapping of heavy particles in the exact potential flow of a vortex pair and its specular image. It is natural to consider whether trapping from the open flow is a robust phenomenon

in the presence of other factors that might not be negligible in realistic situations. Specifically, we show below that the trapping of heavy particles from the open flow also occurs when the particles are subject to gravity, in the presence of noise, and when the potential flow is replaced by a viscous flow obtained from direct simulations of the Navier-Stokes equations. For clarity, we consider each of these three effects separately.

A. Effect of gravity

We use θ to denote the angle between the gravitational field \mathbf{g} and the axis perpendicular to the wall, such that $\mathbf{g} = g(\sin\theta\hat{\mathbf{x}} - \cos\theta\hat{\mathbf{y}})$, and assume that the particles have a small but nonzero settling velocity $\mathbf{g}\tau_p$. In the case of non-vertical walls, the settling velocity is set to zero in a thin layer above the wall in order to account for the finite size of the particles in the particle-wall interactions (e.g. lubrication forces) and prevent particles from crossing the wall in the simulations. In the previous sections, which included no gravity term, this precaution had not been applied since inertia alone cannot lead to the crossing of the symmetry line for small Stokes numbers (i.e. there is no inertial impaction).

Applying the same method used in Sec. II B [32], it can be verified that attracting points still exist in the presence of gravity provided that the settling velocity is not too large. Moreover, it can be shown that in this regime the opening of the internal separatrix Σ_2 is only weakly influenced by gravity and still occurs before the opening of the external separatrix, Σ_3 . The question then is whether particles released in the open flow can cross into the closed component and be captured by the attracting points or possibly by a new attractor. To address this question we investigate the opening of Σ_3 in the presence of gravity.

The equation of motion for a heavy particle in the presence of gravity is obtained by adding the non-dimensional weight force to the drag term. Because we focus on the crossing of the external separatrix Σ_3 , it is convenient to use the external units $V_0 = \Gamma/4\pi L_0$ (for velocities) and L_0 (for lengths) already used in the preceding section. This leads to

$$\varepsilon^2 \text{St} \frac{d^2 \mathbf{X}_p}{dt^2} = \mathbf{V}_f - \frac{d\mathbf{X}_p}{dt} + \tilde{V}_T \hat{\mathbf{g}}, \quad (30)$$

where $\hat{\mathbf{g}}$ is the unit vector in the direction of gravity, \mathbf{V}_f is the non-dimensional fluid velocity corresponding to the streamfunction (22), and $\tilde{V}_T = g\tau_p/V_0$ is the non-dimensional free-fall terminal particle velocity in still fluid. To express that the settling velocity, although small, is sufficiently large to compete against the inertia term (i.e., that the gravity and inertia terms have the same (small) order of magnitude), we set $\tilde{V}_T = \varepsilon^2 \bar{V}_T$, where \bar{V}_T is assumed to be of order unity. Then, expanding the particle velocity in powers of ε leads to Eq. (24) with an extra additive term $\varepsilon^2 \bar{V}_T \hat{\mathbf{g}}$. This is again a rapidly perturbed Hamiltonian system with the same leading order as Eq. (24), but with a different perturbation. The gravity term results in an additive constant term in the Melnikov function:

$$M_g(t_0) = M(t_0) + \bar{V}_T \left(\sin\theta \int_{-\infty}^{\infty} \frac{\partial\psi_0}{\partial x'} dt - \cos\theta \int_{-\infty}^{\infty} \frac{\partial\psi_0}{\partial y'} dt \right), \quad (31)$$

where $M_g(t_0)$ denotes the Melnikov function in the presence of gravity and $M(t_0)$ is the gravity-free Melnikov function given by Eq. (25). The first integral in this equation is the

difference $q_y(-\infty) - q_y(+\infty)$ for a point $\mathbf{q}(t)$ moving on Σ_3 , and is equal to zero. The second integral is equal to $q_x(+\infty) - q_x(-\infty) = -2\sqrt{3}$. We finally obtain

$$M_g(t_0) = 2\sqrt{3}\bar{V}_T \cos \theta - m \text{St} + A(\varepsilon) \left(\sin \frac{2t_0}{\varepsilon^2} - 2\text{St} \cos \frac{2t_0}{\varepsilon^2} \right), \quad (32)$$

where $A(\varepsilon)$ is defined in Eq. (27).

Non-vertical wall. We first assume that $-\pi/2 < \theta < \pi/2$, so that gravity pulls the particles toward the wall (the limit case $\theta = -\pi/2$ is discussed below). It is immediate from Eq. (32) that the constant term due to gravity, $2\sqrt{3}\bar{V}_T \cos \theta$, is positive and hence opposes the constant term due to centrifugal effects, $-m \text{St}$, which is negative. The last term, which is not constant, is a consequence of the unsteady perturbation due to the rotation of the vortex pair. Three kinds of behavior therefore appear:

(i) $M_g(t_0) < 0$ for all t_0 : centrifugal effects dominate over both gravity and unsteadiness. The unstable manifold W^u of the perturbed hyperbolic-saddle point near S_1 wraps around the stable manifold W^s of the hyperbolic-saddle point near S_2 . The dynamics is regular, and particles released outside cannot enter. Particles released inside sufficiently close to Σ_3 will spiral out. This happens when

$$\text{St} > \frac{2\sqrt{3} V_T}{m \varepsilon^3} \cos \theta + \text{St}_{c_3}(\varepsilon) \equiv \text{St}_{c_3}^+(\varepsilon, V_T), \quad (33)$$

where $\text{St}_{c_3}(\varepsilon)$ is the gravity-free critical Stokes number given in Eq. (29).

(ii) $M_g(t_0) > 0$ for all t_0 : gravity dominates over both centrifugal effects and unsteadiness. The manifold W^s now wraps around W^u . The dynamics is regular, but a fraction of the particles released outside can spiral in. This happens when

$$\text{St} < \frac{2\sqrt{3} V_T}{m \varepsilon^3} \cos \theta - \text{St}_{c_3}(\varepsilon) \equiv \text{St}_{c_3}^-(\varepsilon, V_T). \quad (34)$$

(iii) $M_g(t_0)$ has simple zeros: due to the unsteadiness of the flow, a chaotic saddle may exist in the vicinity of Σ_3 (see discussion following Eq. (25)). In either case, the separatrix Σ_3 is necessarily permeable in both directions. In particular, a fraction of the particles released outside penetrate inside after wandering in the heteroclinic tangle. This happens when

$$\text{St}_{c_3}^-(\varepsilon, V_T) < \text{St} < \text{St}_{c_3}^+(\varepsilon, V_T). \quad (35)$$

In the formulae above, the settling velocity \bar{V}_T has been replaced by V_T/ε^3 , where $V_T = g\tau_p/d_0\Omega_0$ is the settling velocity in the unit system (d_0, Ω_0) , which are the units used in the numerical simulations throughout this paper. Note that V_T must be $O(\varepsilon^3)$ for these asymptotic calculations to be valid.

Figure 11 summarizes our numerical verification of the theoretical predictions in Eqs. (33)-(35) for $V_T = 0.003$ and $\theta = 0$ (horizontal wall). In this figure, which was generated employing the same method used to generate Fig. 9, we show all three domains defined by Eqs. (33)-(35) and use circles to represent the parameters (ε, St) above which no particle is observed to cross Σ_3 . The predictions are in good agreement with the numerical results up to $\varepsilon \simeq 0.4$, despite the fact that the numerical calculations were based on using the

exact four-vortex potential flow whereas the theoretical predictions were based on the external perturbative velocity field (22). These results reveal a new regime, where gravity can cause particles released outside to enter the region of closed streamlines without exhibiting (transiently) chaotic dynamics (case (ii)).

We observe that in this regime particles can be permanently trapped by a limit cycle located inside but near Σ_3 . Figure 12 shows two simulations, corresponding respectively to the parameters Q_1 and Q_2 of the trapping diagram of Fig. 11. In each simulation we identified the respective attracting sets for particles released both in the open and in the closed flow by evolving their trajectories for a long period of time. In the case of Q_1 , we observe that a fraction of the particles from the open flow penetrate into the closed component under the sole effect of gravity, as predicted by our theory. These particles are trapped by the limit cycle near Σ_3 (and hence cannot reach the attracting points near the vortices). This limit cycle exists due to the combined effect of gravity and inertia, and also because particles have finite size and are allowed to slip along the wall (i.e., they do not stick to it). As described above, the settling velocity is set to zero in a thin layer above the wall ($0 < y < \delta$). This allows resuspension, which is a key ingredient for the existence of this limit cycle. The exact value of the (small) thickness of the layer is of no importance for the existence of the limit cycle, but it affects its shape slightly (we used $\delta = 0.03$ in the computations of Fig. 12). We have checked that, by decreasing the layer thickness δ , the limit cycle passes closer to the right-side stagnation point, in agreement with the fact that the smaller the thickness, the later the resuspension of the particles will be during their motion along the wall.

Particles from the closed flow, however, can either be driven toward the limit cycle or spiral inside and be captured by the attracting points. In the case of Q_2 , on the other hand, the limit cycle no longer exists and particles from both the closed and the open flow are observed to approach the attracting points. Moreover, plots of particle clouds at intermediate times (not shown) confirm that in this case a heteroclinic tangle exists near Σ_3 , as expected from the Melnikov analysis.

Vertical wall. In the limiting case $\theta = -\pi/2$, vortices move upward with respect to the laboratory frame, and any heavy particle trapped in their neighborhood would be carried against the mean velocity of the fluid *and* against gravity instead of settling down. By considering Eq. (32) with this choice of angle, we observe that gravity does not alter the Melnikov function in this case. Small settling velocities, as considered so far, are therefore unable to affect significantly the dynamics of the particles in the vicinity of the separatrix. In contrast, if the settling velocity is of the order of V_0 , that is $\tilde{V}_T = O(1)$ instead of $O(\varepsilon^2)$ in Eq. (30), then the particle velocity can be expanded as

$$\frac{d\mathbf{X}_p}{dt} = \mathbf{V}_f^0 - \tilde{V}_T \hat{\mathbf{x}} + O(\varepsilon^2). \quad (36)$$

The leading-order particle dynamics now corresponds to the “particle” streamfunction $\psi_p = \psi_0 - y \tilde{V}_T$, which has been widely used as an elementary sedimentation model (see, for example, [56]). One can easily check that this streamfunction has the same general form as ψ_0 , corresponding to a dipole with open streamlines flowing around a closed region, but with a separatrix Σ'_3 smaller than Σ_3 . The separatrix Σ'_3 joins two hyperbolic points, S'_1 and S'_2 , located at $x' = \pm[(6 - \tilde{V}_T)/(2 + \tilde{V}_T)]^{1/2}$ instead of $\pm\sqrt{3}$ (in the external system of units). As long as \tilde{V}_T is not too large, this structure will exist and the conditions leading

to a heteroclinic tangle near Σ'_3 can be derived by a Melnikov analysis similar to the one described in the gravity-free case: one just needs to re-calculate the unperturbed trajectory $\mathbf{q}(t)$ on Σ'_3 . To check that attracting points still exist, we have performed simulations in the case $\tilde{V}_T = 0.28$, $St = 0.006$ and $\varepsilon = 0.4$ (Fig. 13). The simulations confirm that such points do exist and that they capture particles coming from the open portion of the flow.

B. Effect of viscosity

The calculations described in the above sections concern flows whose velocity fields are determined on the basis of the inviscid fluid approximation. That is, viscosity was assumed to be important only at scales comparable to or smaller than the particle diameter. However, when the flow Reynolds number is only moderately large, viscosity is expected to play an important role also at scales of the order of the distance between vortices. At those scales it leads to vortex merging, which eventually destroys the co-rotating vortex pairs. Vortex merging starts when, due to viscous diffusion, the linear size of the vortex cores reaches a critical value of the order of the initial distance between the vortices (see, for example, [14] and references therein, or [12] for vortex merging in an external strain flow). We hypothesize that, if the time scale of viscous diffusion is much larger than the turnover time of the vortices, trapping of particles will occur as predicted by the potential flow theory (although only until vortex coalescence takes place).

To test this hypothesis, we have performed a series of numerical simulations of the two-dimensional Navier-Stokes equations with an initial vortex pair parallel to the x -axis, composed of two identical Lamb-Oseen vortices with individual strength Γ and separated by a distance $2d_0$. In addition, “mirror” vortices with strength $-\Gamma$ are placed symmetrically with respect to the x -axis, at a distance $2L_0$ below the first pair, which causes the vortex system to move in the x -direction. Due to viscosity, the mirror vortices in this case do not represent the effect of a wall, but they are added to create an open flow that corresponds to the viscous analogue of the flow system considered in the previous sections. In the following simulations, one million passive and collisionless particles are injected at random initial positions in a region covering the upper vortices. Then the particle and the fluid equations are solved for several turnover times, starting at $t = 0$, until vortex merging occurs. We use the same non-dimensionalization for length and time scales used in our study of the internal flow, except that here d_0 and Ω_0 are the *initial* half-distance and angular velocity, respectively. The corresponding Reynolds number of the flow, $Re = \Omega_0 d_0^2 / \nu$ (where ν is the kinematic viscosity), is equal to 400 and the Stokes number of the particles is $St = 0.07$.

The flow domain is a two-dimensional periodic box, which allows us to use a Fourier series decomposition in both x and y . A second-order Adams-Bashforth algorithm is employed for the time integration of both the fluid and the particle equations, with a time-step calculated to satisfy the Courant-Friedrichs-Lewy condition [11]. The fluid velocity at the particle position is interpolated by means of Shepard’s method (inverse distance weighted interpolation). Using these techniques, we implemented two runs, corresponding to $\varepsilon = 0.4$ and $\varepsilon = 0.2$, respectively. In the former case, the box size is equal to $15d_0$ in both the x and y directions, and 512×512 Fourier modes are used. In the latter case, the size of the box was increased to $30d_0$ in the y -direction to avoid spurious self-interactions due to the periodicity of the box for small ε .

Figure 14(a) shows the particle cloud for the $\varepsilon = 0.4$ run at time $t = 7.1$. Two clusters of particles are visible near the vortices (marked blue and red blobs). One can check that the particles follow the vortices until merging takes place and hence are temporarily trapped. The initial positions of the colored particles are indicated with the corresponding colors in Fig. 14(d). The overall shape of this basin is roughly comparable to that of the vortex pair of the inviscid fluid (Fig. 6(e)). This suggests that the clustering of particles seen in the Navier-Stokes simulation has the same dynamical origin as the trapping phenomenon studied in Secs. II and III. The basin boundary of Fig. 14(d) is smooth, however, since it corresponds to short simulation times. Figures 14(b) and 14(c) show particle clouds (at $t = 12.4$ and $t = 19.4$ respectively), which correspond to two typical structures of the vorticity field (eight shape and spiral shape). The initial positions of the trapped particles are indicated in Figs. 14(e) and 14(f). The basin boundaries now display a more filamentary structure, rather similar to the potential flow case (Fig. 6(e)). However, this structure cannot show very thin filaments, as viscosity causes vortex merging. Indeed, the spiral structure wrapped around the trapped particles (dashed lines in Fig. 14(c)) is temporary and is eventually smoothed out by viscous diffusion, which centrifugates the particles away.

The inviscid-fluid calculations of Sec. III also suggest that the basin boundary should be smooth when $\varepsilon = 0.2$ (Fig. 6(d)). We have checked whether this could be observed also in the viscous case by setting $\varepsilon = 0.2$ in our numerical calculations, corresponding to a distance $2/\varepsilon = 10$ between the vortex pairs. Figure 15 shows the particle cloud at three different times (left panels) corresponding to the three typical stages of vortex interaction, together with the initial positions of the trapped particles (right panels). In this case the basins of attraction have smooth boundaries, as no filamentation is visible, and are therefore very similar to the portraits of Figs. 6(a) and 6(d). This supports the conclusion that, to a good approximation, the potential flow theory correctly predicts the dynamics of heavy particles in this flow until vortex merging starts to occur.

C. Effect of noise

In the laboratory frame, the dimensional form of the equation of motion for a heavy particle under thermal noise is [18]

$$\frac{d^2 \mathbf{X}_p}{dt^2} = \frac{1}{\tau_p} \left(\mathbf{V}_f - \frac{d\mathbf{X}_p}{dt} \right) + \mathbf{f}(t), \quad (37)$$

where $\mathbf{f}(t)$ is the random force per unit of mass of the particle. The components of this force are assumed to be of zero mean, Gaussian, and delta-correlated in time:

$$\langle f_i(t) f_j(t') \rangle = q \delta_{ij} \delta(t - t'), \quad i, j \in \{x, y\}, \quad (38)$$

where $\langle \cdot \rangle$ denotes average and q is the strength of the force. The fluctuation dissipation theorem allows relating q to the diffusion coefficient \mathcal{D} as $q = 2\mathcal{D}/\tau_p^2$ [18].

Using the characteristic velocity magnitude and the characteristic length of the fluid flow, we can write Eq. (37) in dimensionless form:

$$\frac{d^2 \mathbf{X}_p}{dt^2} = \frac{1}{St} \left(\mathbf{V}_f - \frac{d\mathbf{X}_p}{dt} \right) + \sqrt{2\Delta} \xi(t), \quad (39)$$

where $\Delta = 1/(\text{St}^2\text{Pe})$ is the non-dimensional noise strength, $\text{Pe} = \Omega_0 d_0^2/\mathcal{D}$ is the Péclet number, and $\xi(t)$ is a zero-mean normalized Gaussian white noise.

We have explored numerically the possibility of trapping in the presence of noise. Figure 16 shows the capture of heavy particles released in the open component of the flow and whose motion is described by Eq. (39). A systematic account of the effects of noise for different Stokes numbers is summarized in Fig. 17, where we show as a function of $1/\text{Pe}$ the fraction of particles released in the open flow that are trapped. The axis $1/\text{Pe} = 0$ corresponds to the noiseless case. Remarkably, as the noise intensity (i.e., $1/\text{Pe}$) increases from zero, the percentage of particles trapped also increases; this percentage only starts to decrease at sufficiently large noise intensities. We therefore conclude that trapping is robust with respect to noise, and can in fact be enhanced by noise. The enhancement of particle trapping at intermediate noise levels may be due to the fact that noise can cause inertial particles to cross the separatrix Σ_3 even when the inertia of the particles is too large for this to occur in the absence of noise. In contrast, larger noise intensities cause the particles to move erratically and eventually inhibit trapping.

VI. CONCLUSIONS

The analytical calculations presented in this paper show that heavy particles released in the upstream flow of a vortex pair (and its specular image, modeled as a wall) can be trapped by point attractors moving with the vortices. The stability of these points is determined by a balance between the centrifugal force (due to the rotation of vortices around each other) and the inward drag. It is observed that the dynamics of the inertial particles can become transiently chaotic, as long as the distance between the vortex pairs (or, equivalently, the distance to the wall) is below a critical value that depends on the particle Stokes number. This chaotic behavior results in fractal basin boundaries for the attracting points, which was verified for specific parameter choices by showing that the fractal dimension of the basin boundaries becomes larger than three in the four-dimensional phase space as soon as our analytical criterion predicting a heteroclinic tangle near the separatrix Σ_2 is fulfilled.

This metamorphosis of the basin boundaries has a dramatic consequence for particle dynamics: one can no longer easily predict which particles will be captured by a given attracting point and which particles will be captured by the other attracting point or, when the external separatrix can also be crossed, go to infinity. That is, due to transient chaos and the fractal basin boundaries that come with it, the particle dynamics exhibits final state sensitivity. Moreover, particles injected at different locations of the flow domain can undergo mixing in the neighborhood of the chaotic set prior to converging to their final states (either of the attracting points or infinity). In other words, particles are mixed before being either trapped or centrifuged away.

For an observer translating with the vortices, the flow consists of a portion formed by closed streamlines and a portion formed by open streamlines further away from the vortices, with separatrix Σ_3 at the boundary between them. The trapping of heavy particles released in the open part of the flow requires that both the separatrix Σ_3 and the separatrix Σ_2 of the flow be permeable with respect to the particles. We have shown that, in order to become permeable to heavy particles, in the absence of gravity the separatrices have to not only break but also give rise to heteroclinic tangles, which occurs when the flow unsteadiness

induced by the wall is sufficiently strong. Therefore, the wall has a double role: it not only causes the flow to be open, but it also allows particles to cross the separatrices and eventually be trapped in the neighborhood of the vortices. We note that, while inertia is necessary for the formation of attractors, the larger the Stokes number the more difficult it is for the separatrices to be crossed (i.e., closer proximity to the wall is required).

The theory we established using perturbative velocity fields allowed us to generate a global trapping diagram (Fig. 9), which can be used to predict particle trapping in the $St-\varepsilon$ plane for small particle Stokes number St and small inverse distance to the wall ε . Comparisons between this diagram and numerical simulations using the exact four-vortex system are excellent. This analysis reveals the mechanism underlying the trapping of aerosols from the open flow in this system. In the absence of gravity, it is the emergence of heteroclinic tangles induced by the wall that is responsible for trapping from the open flow. Further analysis demonstrated that, in the presence of gravity, trapping from the open flow is also possible without the formation of a heteroclinic tangle in the vicinity of the external separatrix.

The robustness of particle trapping from the open flow was verified by considering systematically the effects of gravity, noise, and viscosity. Trapping persists in the presence of gravity for any orientation of the wall, provided that the settling velocity is not too large. In particular, for a non-vertical wall the perturbative analysis could be readily generalized, and three kinds of behavior were shown to exist (summarized in the trapping diagram of Fig. 11 for a horizontal wall). In this case gravity can cause the particles to cross the external separatrix in a non-chaotic manner, and be trapped permanently by a limit cycle next to it. This behavior, which requires that particles be allowed to slip on the wall (no deposition), is a form of non-chaotic trapping from the open flow. The limit cycle was observed to coexist with the attracting points near the vortices: particles released in the closed portion of the flow can either spiral in toward one of the attracting points or spiral out toward the limit cycle.

Numerical simulations of the Navier-Stokes equations showed that, when the fluid is viscous, the attracting points persist until vortex merging starts to occur. When vortex coalescence takes place, the attracting points vanish and particles are centrifuged away, as expected. But prior to the vortex merging, the overall structure of the “attraction basins” is rather similar to the basins in the inviscid case, provided that the flow Reynolds number is large enough. Finally, trapping also persists in the presence of noise. Using the exact potential flow, we observed that Brownian heavy particles can be trapped for at least several tens of periods of the background fluid flow, provided that the Péclet number is sufficiently large.

The particles in this study were taken to be sufficiently dilute so that their effect on the fluid could be neglected (“one-way coupling”). This assumption is not valid for large particle loadings, especially in zones where particles accumulate. Inertial particles have been shown to influence vortex pairing in mixing layers [42, 58]. It could therefore be interesting to extend this study to investigate the effect of the dispersed phase on the vortex pairing phenomenon considered here. In the same vein, particle collisions, which were neglected in the present study, are known to influence the trapping process [40, 61]. In addition, it would be interesting to consider particles with density comparable with the fluid density and investigate the effect of the Boussinesq-Basset, added-mass, and lift forces on the trapping process (see, for example, [16], [51], [17], and [19]). Such an extended analysis of inertial particle dynamics is among the topics for future exploration that we hope our results will

encourage researchers to pursue.

ACKNOWLEDGEMENT

The authors thank I. Fouxon for useful discussions and E. Hicks for providing feedback on the manuscript. This research was supported by the National Science Foundation through Grant No. PHY-1001198. R.D.V. acknowledges financial support from CNPq (Brazil).

-
- [1] ANGILELLA, J.-R. 2010 Dust trapping in vortex pairs. *Physica D* **239**, 1789–1797.
 - [2] ANGILELLA, J.-R. 2011 Asymptotic properties of wall-induced chaotic mixing in point vortex pairs. *Phys. Fluids* **23**, 113602.
 - [3] ANTONSEN, T.M. & OTT, E. 1991 Multifractal power spectra of passive scalars convected by chaotic fluid-flows. *Phys. Rev. A* **44**, 851–857.
 - [4] ARNOLD, V. 1965 Sur la topologie des écoulements stationnaires des fluides parfaits. *C. R. Acad. Sci. Paris A* **261**, 17–20.
 - [5] BABIANO, A., CARTWRIGHT, J. H. E., PIRO, O. & PROVENZALE, A. 2000 Dynamics of a small neutrally buoyant sphere in a fluid and targeting in Hamiltonian systems. *Phys. Rev. Lett.* **84**, 5764–5767.
 - [6] BALKOVSKY, E., FALKOVICH, G. & FOUXON, A. 2001 Intermittent distribution of inertial particles in turbulent flows. *Phys. Rev. Lett.* **86**, 2790–2793.
 - [7] BARGE, P. & SOMMERIA, J. 1995 Did planet formation begin inside persistent gaseous vortices? *Astron. Astrophys.* **295**, L1–L4.
 - [8] BEC, J. 2003 Fractal clustering of inertial particles in random flows. *Phys. Fluids* **15**, L81–L84.
 - [9] BENCZIK, I. J., TOROCZKAI, Z. & TÉL, T. 2002 Selective sensitivity of open chaotic flows on inertial tracer advection: Catching particles with a stick. *Phys. Rev. Lett.* **89**, 164501.
 - [10] BENCZIK, I. J., TOROCZKAI, Z. & TÉL, T. 2003 Advection of finite-size particles in open flows. *Phys. Rev. E* **67**, 036303.
 - [11] CANUTO, C., HUSSAINI, M. Y., QUARTERONI, A. & ZANG, T. A. 1988 *Spectral Methods in Fluid Dynamics*. Springer-Verlag, Berlin.
 - [12] CARTON, X., MAZE, G. & LEGRAS, B. 2002 A two-dimensional vortex merger in an external strain field. *J. Turbul.* **3**, 045.
 - [13] CARTWRIGHT, J., FEUDEL, U., KAROLYI, G., DE MOURA, A., PIRO, O. & TEL, T. 2010 Dynamics of finite-size particles in chaotic fluid flows. In *Nonlinear Dynamics and Chaos: Advances and Perspectives* (ed. M. THIEL). Springer-Verlag, Berlin.
 - [14] CERRETELLI, C. & WILLIAMSON, C. H. K. 2003 The physical mechanism for vortex merging. *J. Fluid Mech.* **475**, 41–77.
 - [15] CUZZI, J. N., HOGAN, R. C., PAQUE, J. M. & DOBROVOLSKIS, A. R. 2001 Size-selective concentration of chondrules and other small particles in protoplanetary nebula turbulence. *Astrophys. J.* **546**, 496–508.
 - [16] DAITCHE, A. & TÉL, T. 2011 Memory effects are relevant for chaotic advection of inertial particles. *Phys. Rev. Lett.* **107**, 244501.
 - [17] DE LILLO, F., CECCONI, F., LACORATA, G. & VULPIANI, A. 2008 Sedimentation speed of inertial particles in laminar and turbulent flows. *Europhys. Lett.* **84**, 40005.

- [18] DROSSINOS, Y. & REEKS, M. W. 2005 Brownian motion of finite-inertia particles in a simple shear flow. *Phys. Rev. E* **71**, 031113.
- [19] DROTOS, G. & TÉL, T. 2011 Chaotic saddles in a gravitational field: The case of inertial particles in finite domains. *Phys. Rev. E* **83**, 056203.
- [20] DUNCAN, K., MEHLIG, B., OSTLUND, S. & WILKINSON, M. 2005 Clustering by mixing flows. *Phys. Rev. Lett.* **95**, 240602.
- [21] FALKOVICH, G., GAWEDSKI, K. & VERGASSOLA, M. 2001 Particles and fields in fluid turbulence. *Rev. Mod. Phys.* **73**, 913–975.
- [22] FALKOVICH, G., FOUXON, A. & STEPANOV, M. G. 2002 Acceleration of rain initiation by cloud turbulence. *Nature* **419**, 151–154.
- [23] FESSLER, J. R., KULICK, J. D. & EATON, J. K. 1994 Preferential concentration of heavy particles in a turbulent channel flow. *Phys. Fluids* **6**, 3742–3749.
- [24] FOUXON, I. 2012 Distribution of particles and bubbles in turbulence at a small Stokes number. *Phys. Rev. Lett.* **108**, 134502.
- [25] GATIGNOL, R. 1983 The Faxén formulae for a rigid particle in an unsteady non-uniform Stokes flow. *J. Méc. Théor. Appl.* **1**, 143–160.
- [26] GAUTERO, J.L. 1985 Chaos lagrangien pour une classe d’écoulements de Beltrami. *C. R. Acad. Sci. S. II.* **301**(15), 1095–1098.
- [27] GELFREICH, V. G. 1997 Melnikov method and exponentially small splitting of separatrices. *Physica D* **101**, 227–248.
- [28] GRASSBERGER, P. 1986 Estimating the fractal dimensions and entropies of strange attractors. In *Chaos* (ed. A.V. HOLDEN). Manchester University Press, Manchester.
- [29] GUCKENHEIMER, J. & HOLMES, P. 1983 *Nonlinear oscillations, dynamical systems, and bifurcations of vector fields*. Springer, New York.
- [30] HALLER, G. & SAPSIS, T. 2008 Where do inertial particles go in fluid flows? *Physica D* **237**, 573–583.
- [31] HALLER, G. & SAPSIS, T. 2010 Localized instability and attraction along invariant manifolds. *SIAM J. Applied Dynamical Systems* **9**(2), 611–633.
- [32] IJZERMANS, R. H. A. & HAGMEIJER, R. 2006 Accumulation of heavy particles in N-vortex flow on a disk. *Phys. Fluids* **18**, 063601.
- [33] LIU, S.-J., WEI, H.-H., HWANG, S.-H. & CHANG, H.-C. 2010 Dynamic particle trapping, release, and sorting by microvortices on a substrate. *Phys. Rev. E* **82**, 026308.
- [34] MCLAUGHLIN, J. B. 1988 Particle size effects on lagrangian turbulence. *Phys. Fluids* **31**, 2544–2553.
- [35] MAXEY, M. R. 1987 The motion of small spherical particles in a cellular flow field. *Phys. Fluids* **30**, 1915–1928.
- [36] MAXEY, M. R. 1987 The gravitational settling of aerosol particles in homogeneous turbulence and random flow fields. *J. Fluid Mech.* **174**, 441–465.
- [37] MAXEY, M. R. & CORRSIN, S. 1986 Gravitational settling of aerosol particles in randomly oriented cellular flow fields. *J. Atmos. Sci.* **43**, 1112–1134.
- [38] MAXEY, M. R. & RILEY, J. J. 1983 Equation of motion for a small rigid sphere in a non uniform flow. *Phys. Fluids* **26**, 883–889.
- [39] MAZE, G., CARTON, X. & LAPEYRE, G. 2004 Dynamics of a 2D vortex doublet under external deformation. *Regul. Chaotic Dyn.* **9**, 477–497.
- [40] MEDRANO, R. O., MOURA, A., TEL, T., CALDAS, I. L. & GREBOGI, C. 2008 Finite-size particles, advection, and chaos: A collective phenomenon of intermittent bursting. *Phys. Rev. E* **78**, 056206.
- [41] MEHLIG, B., WILKINSON, M., DUNCAN, K., WEBER, T. & LJUNGGREN, M. 2005 Aggregation of inertial particles in random flows. *Phys. Rev. E* **72**, 051104.

- [42] MEIBURG, E., WALLNER, E., PAGELLA, A., RIAZ, A., HARTEL, C. & NECKER, F. 2000 Vorticity dynamics of dilute two-way-coupled particle-laden mixing layers. *J. Fluid Mech.* **421**, 185–227.
- [43] MEYER, C. J. & DEGLON, D. A. 2011 Particle collision modeling - A review. *Miner. Eng.* **24**, 719–730.
- [44] MICHAELIDES, E. E. 1997 The transient equation of motion for particles, bubbles, and droplets. *J Fluid Eng.-T. Asme* **119**, 233-247.
- [45] OLLA, P. 2010 Preferential concentration versus clustering in inertial particle transport by random velocity fields. *Phys. Rev. E* **81**, 016305.
- [46] OTTINO, J. 1989 *The kinematics of mixing: stretching, chaos and transport*. Cambridge University Press, Cambridge, UK.
- [47] PASQUERO, C., PROVENZALE, A. & SPIEGEL, E. A. 2003 Suspension and fall of heavy particles in random two-dimensional flow. *Phys. Rev. Lett.* **91**, 054502.
- [48] PUSHKIN, D. O., MELNIKOV, D. E. & SHEVTSOVA, V. M. 2011 Ordering of Small Particles in One-Dimensional Coherent Structures by Time-Periodic Flows. *Phys. Rev. Lett.* **106**, 234501.
- [49] ROM-KEDAR, V., LEONARD, A. & WIGGINS, S. 1990 An analytical study of transport, mixing and chaos in an unsteady vortical flow. *J. Fluid Mech.* **214**, 347–394.
- [50] RUBIN, J., JONES, C. K. R. T. & MAXEY, M. 1995 Settling and asymptotic motion of aerosol particles in a cellular flow field. *J. Nonlinear Sci.* **5**, 337–358.
- [51] SAPSIS, T. & HALLER, G. 2008 Instabilities in the dynamics of neutrally buoyant particles. *Phys. Fluids* **20**, 017102.
- [52] SAPSIS, T. & HALLER, G. 2009 Inertial particle dynamics in a hurricane. *J. Atmosph. Sci.* **66**, 2481–2492.
- [53] SAPSIS, T. & HALLER, G. 2010 Clustering criterion for inertial particles in two-dimensional time-periodic and three-dimensional steady flows. *Chaos* **20**, 017515.
- [54] SHAW, R. A. 2003 Particle-turbulence interactions in atmospheric clouds. *Annu. Rev. Fluid Mech.* **35**, 183–227.
- [55] SQUIRES, K. D. & EATON, J. K. 1991 Preferential concentration of particles by turbulence. *Phys. Fluids* **3**, 1169–1178.
- [56] STOMMEL, H. 1949 Trajectories of small bodies sinking slowly through convection cells. *J. Marine Res.* **8**, 24–29.
- [57] VILELA, R. D. & MOTTER, A. E. 2007 Can aerosols be trapped in open flows? *Phys. Rev. Lett.* **99**, 264101.
- [58] WALLNER, E. & MEIBURG, E. 2002 Vortex pairing in two-way coupled, particle laden mixing layers. *Int. J. Multiphas. Flow* **28**, 325–346.
- [59] WILKINSON, M., MEHLIG, B., OSTLUND, S. & DUNCAN, K. P. 2007 Unmixing in random flows. *Phys. Fluids* **19**, 113303.
- [60] WILKINSON, M., MEHLIG, B. & GUSTAVSSON, K. 2010 Correlation dimension of inertial particles in random flows. *Europhys. Lett.* **89**, 50002.
- [61] ZAHNOW, J. C. & FEUDEL, U. 2009 What determines size distributions of heavy drops in a synthetic turbulent flow? *Nonlinear Proc. Geoph.* **16**, 677–690.

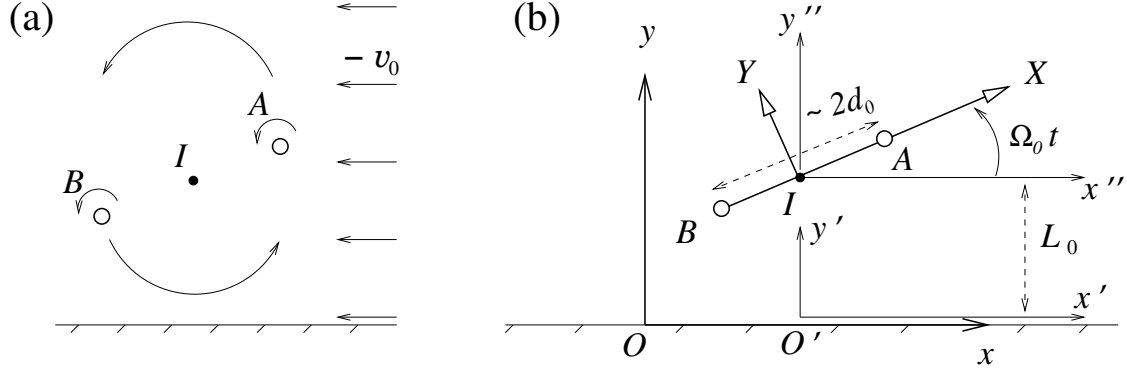


FIG. 1. Sketch of the vortex pair considered in this study. (a) Symbols A and B denote co-rotating point vortices of same strength Γ . To first order, the center of vorticity I moves to the right with constant velocity v_0 equal to $2\varepsilon\Omega_0 d_0 \equiv \Gamma/(2\pi L_0)$. (b) The vortices are separated from each other by an average distance $2d_0$, and I is at a distance L_0 from a wall (which can be interpreted as a symmetry line) represented by the Ox axis. Here, xOy is a coordinate system of the laboratory frame, $x'O'y'$ and $x''Iy''$ are coordinate systems of the non-rotating frame translating with velocity v_0 , and XIY is a coordinate system of the rotating frame.

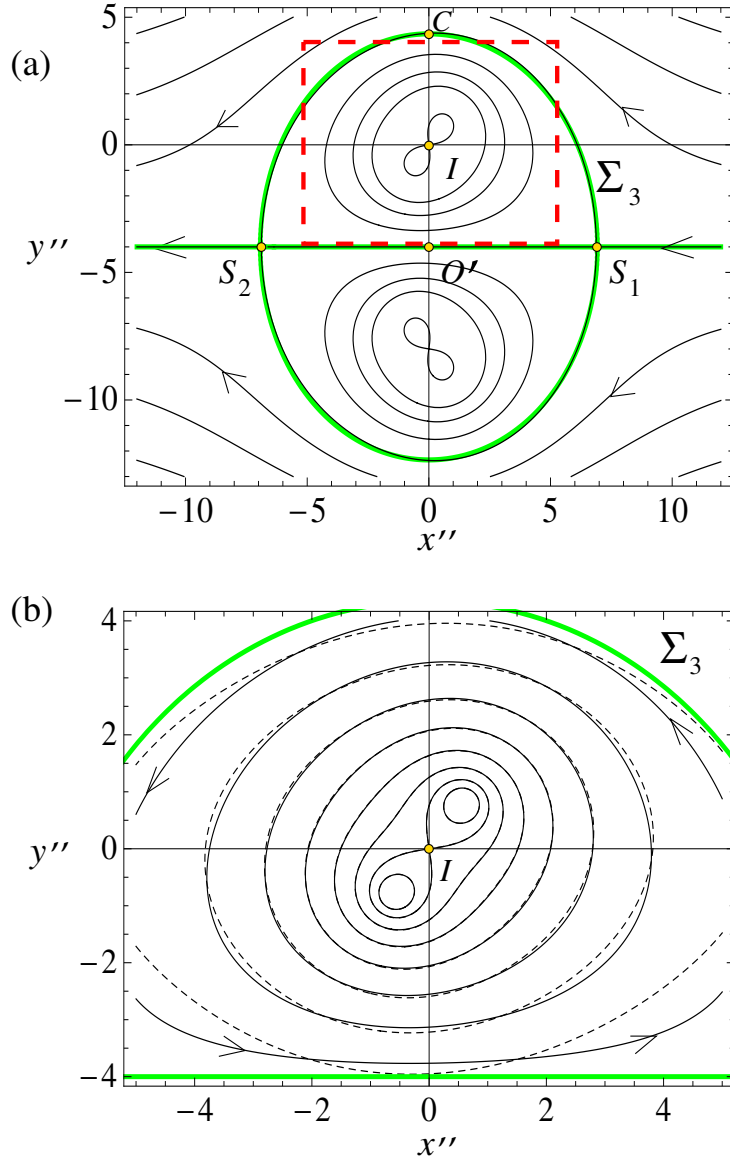


FIG. 2. Streamlines of the vortex system. (a) Streamlines of the exact four-vortex potential flow in the frame translating with the vortices for $\varepsilon = 0.25$. The bold curve (green) corresponds to the separatrix Σ_3 (and its mirror image) between closed and open streamlines, which is associated with the fixed points S_1 and S_2 . (b) Magnification of the dashed rectangle of panel (a), showing the internal perturbative flow described by Eq. (2) (dashed lines) on top of the exact potential flow (solid lines). In both panels, the streamfunction isolines are taken at a particular time and are equispaced.

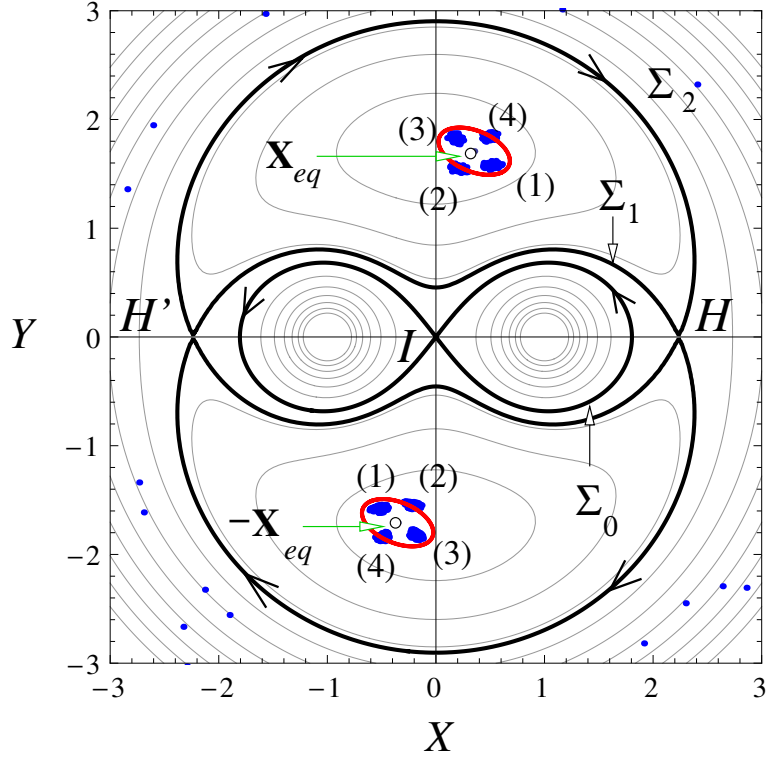


FIG. 3. Periodic attractors in the rotating reference frame. The blue dots correspond to the simulated final positions of heavy particles with $St = 0.1$ transported by the flow defined by $\varepsilon = 1/3$. The red ellipses (solid lines) correspond to the analytical prediction in Eq. (15) for attractors projected on the physical space. The simulations assume that the particles have initial velocity equal to the fluid velocity and are initially uniformly distributed in the region shown. The numbers (i) next to the particle clusters indicate the time $t_f - (\frac{4-i}{4})\pi$ ($i = 1, \dots, 4$) at which the particles are observed, where the final time $t_f = 14 \times 2\pi$ corresponds to 14 turnover times of the vortex pair. Particles away from the attracting points correspond to initial conditions outside the basins of attraction. Regular lines represent equispaced streamlines, bold lines represent the separatrices Σ_0 , Σ_1 , and Σ_2 , and open circles indicate the stable equilibrium points $\pm \mathbf{X}_{eq}$ in the limit of vanishing ε (i.e., in the absence of the wall).

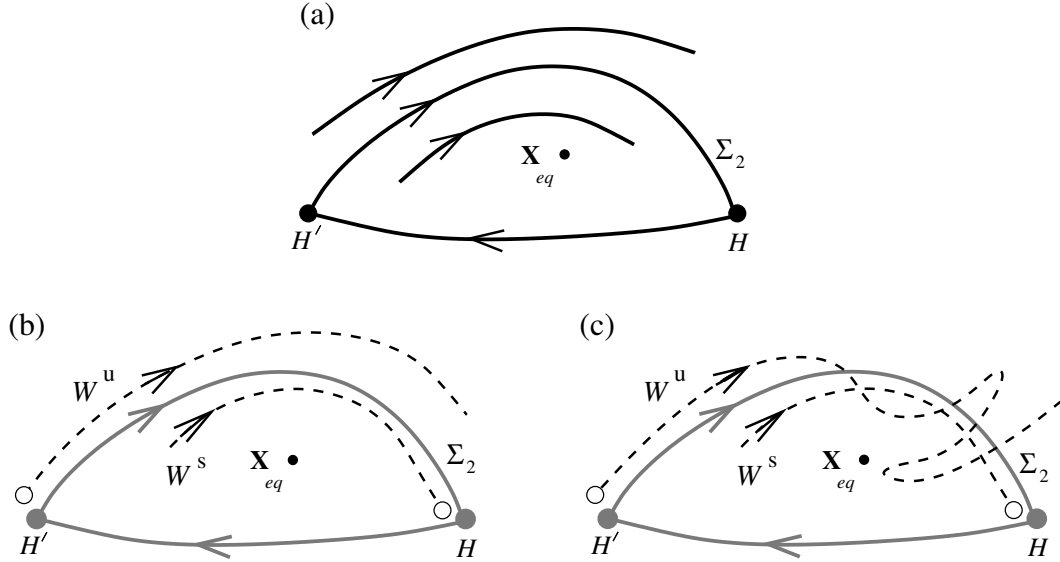


FIG. 4. Sketch of impact of inertia and wall on the separatrix Σ_2 . (a) The separatrix Σ_2 in the absence of both particle inertia and wall-induced flow unsteadiness. In this case, the stable manifold W^s of H and unstable manifold W^u of H' coincide with the separatrix. (b) Separation between the stable and unstable manifolds induced by particle inertia, when the inertia dominates over the wall effect. In this case, the manifolds do not intersect each other, but particles outside W^s cannot reach the attracting point \mathbf{X}_{eq} because the particle-velocity field between W^s and W^u spirals outward. (c) Transverse intersections between the stable and unstable manifolds induced by the wall, when the wall dominates over the particle inertia. In this case, the particles from outside that are in the lobes bounded by W^u can now cross W^s and as a result they can in principle approach the attracting point.

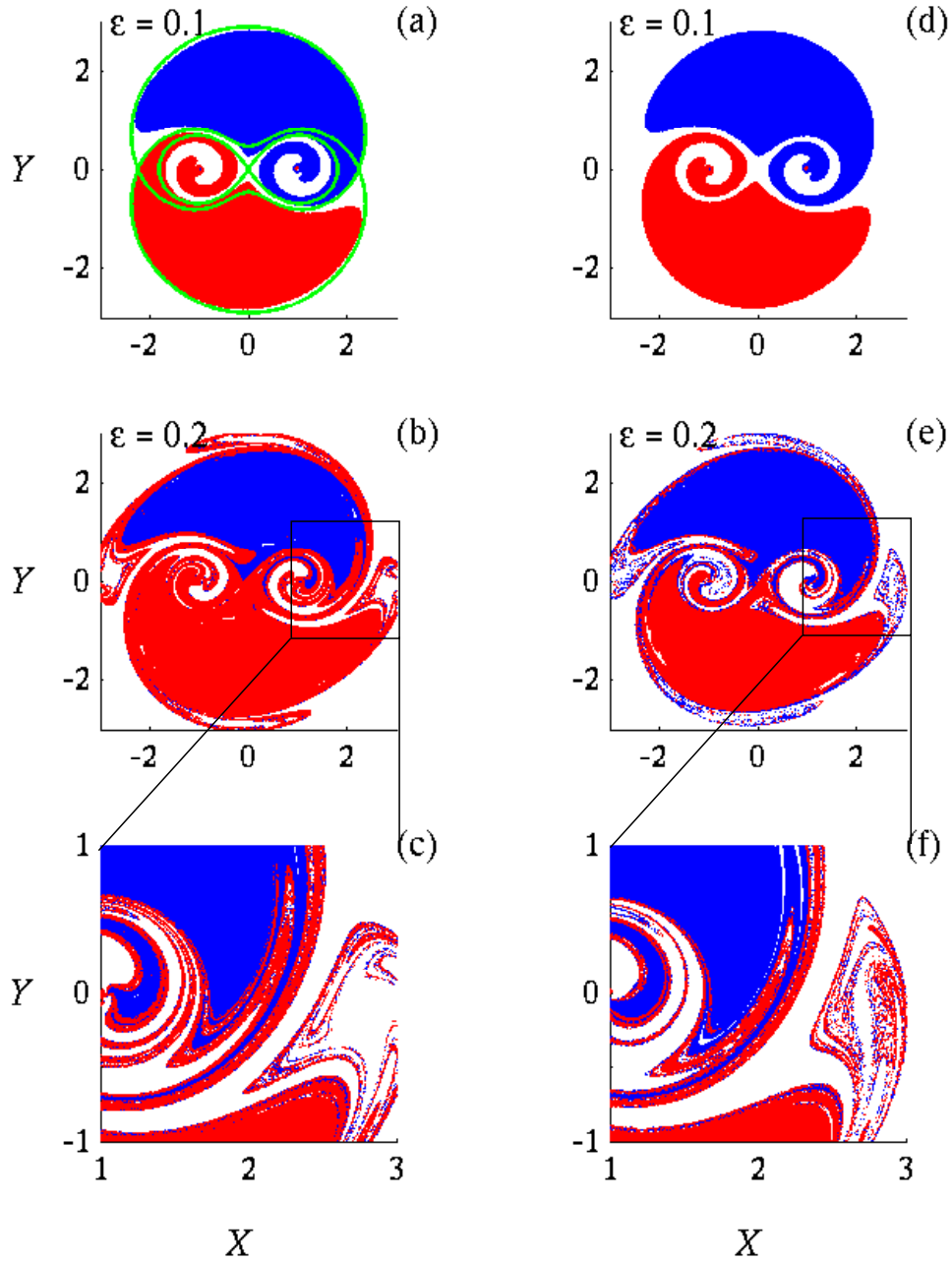


FIG. 5. Smooth versus fractal basin boundaries. Blue and red indicate the basins of attraction associated with the two periodic attractors for heavy particles for $St = 0.02$ and initial velocity equal to the fluid velocity. (a-c) Perturbative velocity field simulations. (d-f) Exact potential flow simulations. The basin boundaries are smooth when the distance from the center of vorticity to the wall is large (a, d) and become fractal as this distance is reduced (b, e). Panels (c) and (f) are magnifications of the rectangles shown in panels (b) and (e), respectively. The continuous (green) lines in panel (a) correspond to the separatrices defined in Fig. 3.

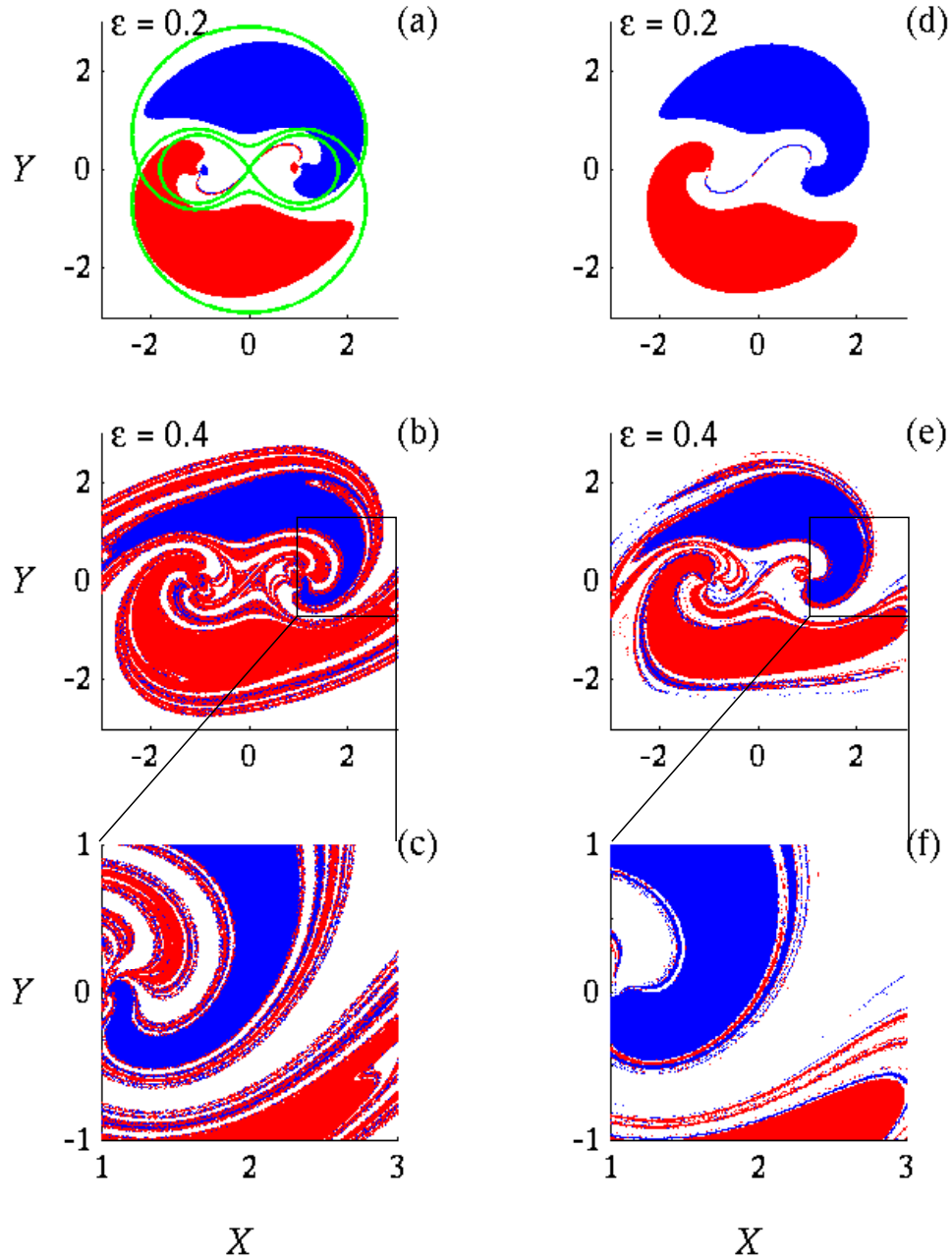


FIG. 6. Counterpart of Fig. 5 for $St = 0.07$. The differences between the perturbative velocity field simulations in panels (a-c) and the exact potential flow simulations in panels (d-f) are now more noticeable because ε is larger. The transition from smooth to fractal is in both cases in good agreement with the theoretical prediction from Eq. (21).

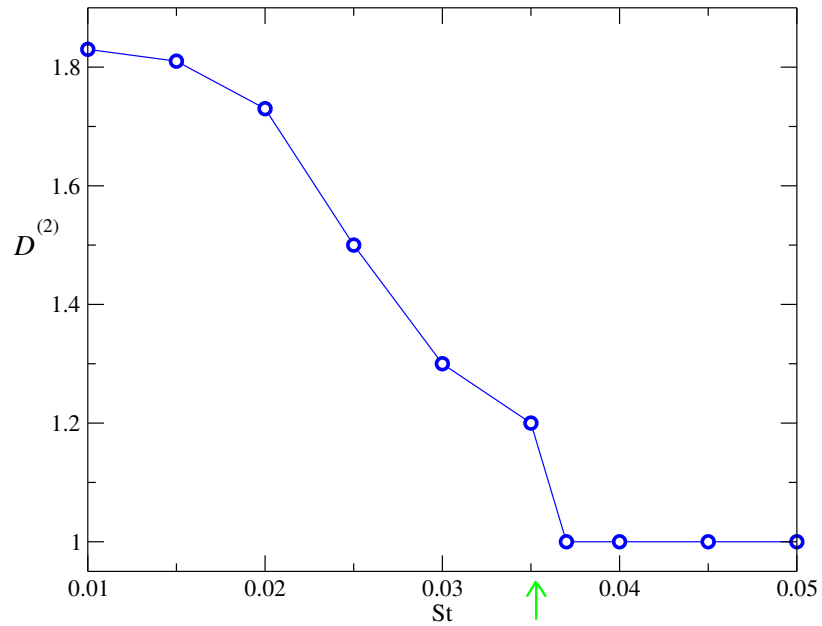


FIG. 7. Transition from smooth to fractal basin boundary as particle inertia is increased. Basin boundary dimension as a function of the Stokes number for $\varepsilon = 0.2$. The basin boundary is fractal when $St \lesssim St_{c_2} = 0.0352$, in agreement with our theory (green arrow). The symbols correspond to numerical simulations and the continuous line is a reference to guide the eye.

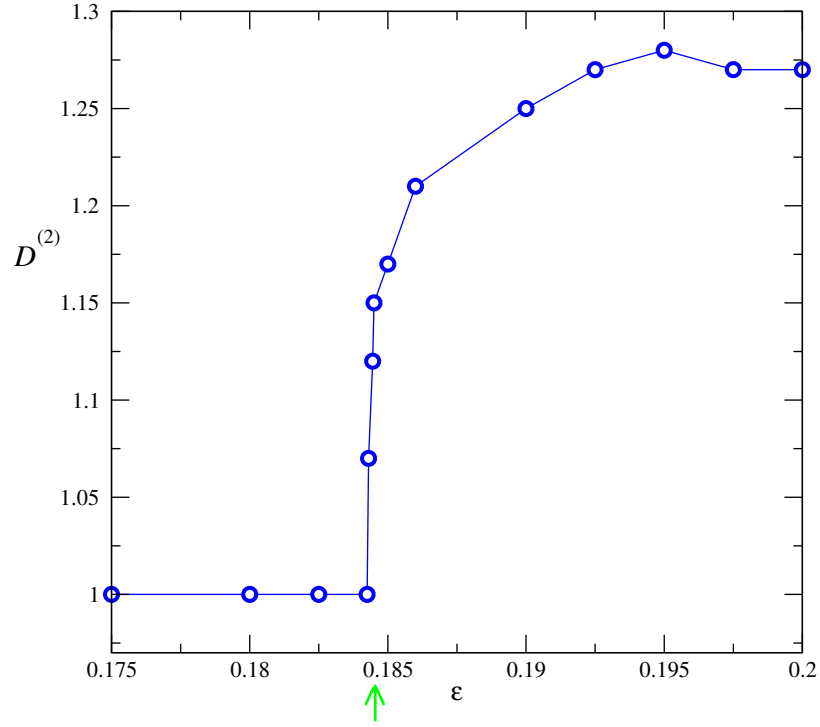


FIG. 8. Transition to fractal basin boundary as the perturbation of the flow by the wall is increased. The symbols correspond to numerical simulations of the basin boundary dimension as a function of ϵ for $St = 0.03$. At $\epsilon \approx 0.1846$ the basin boundary ceases being smooth, in quantitative agreement with our theory (green arrow). The continuous line is a reference to guide the eye.

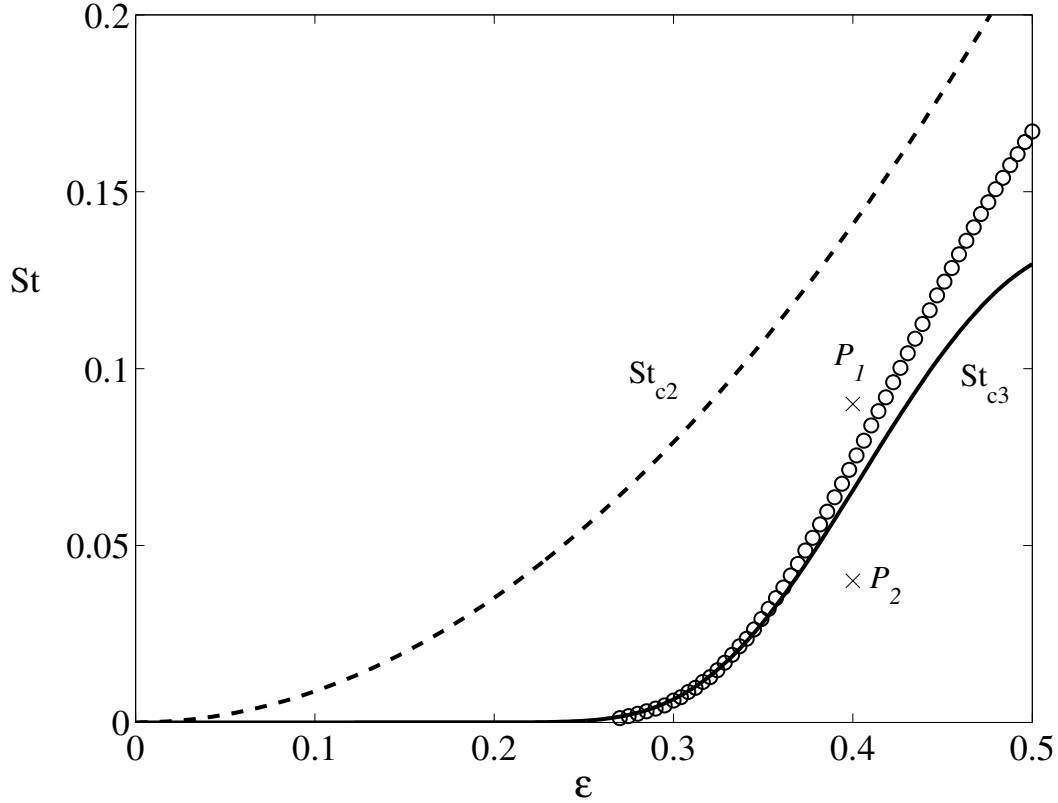


FIG. 9. Global trapping diagram for heavy particles in the absence of gravity. The dashed curve is the theoretical critical Stokes number St_{c_2} for the opening of the internal separatrix Σ_2 (Eq. (21)), whereas the continuous curve is the theoretical critical Stokes number St_{c_3} for the opening of the external separatrix Σ_3 (Eq. (29)). These curves define three regions according to whether external particles can cross the corresponding separatrix. Circles represent a numerical verification of St_{c_3} based on simulations of the exact potential flow. Parameter points (ε, St) above the circles (such as P_1) correspond to scenarios in which particles released in the open component of the flow do not cross Σ_3 , while points below the circles (such as P_2) correspond to scenarios in which a fraction of them do cross inside.

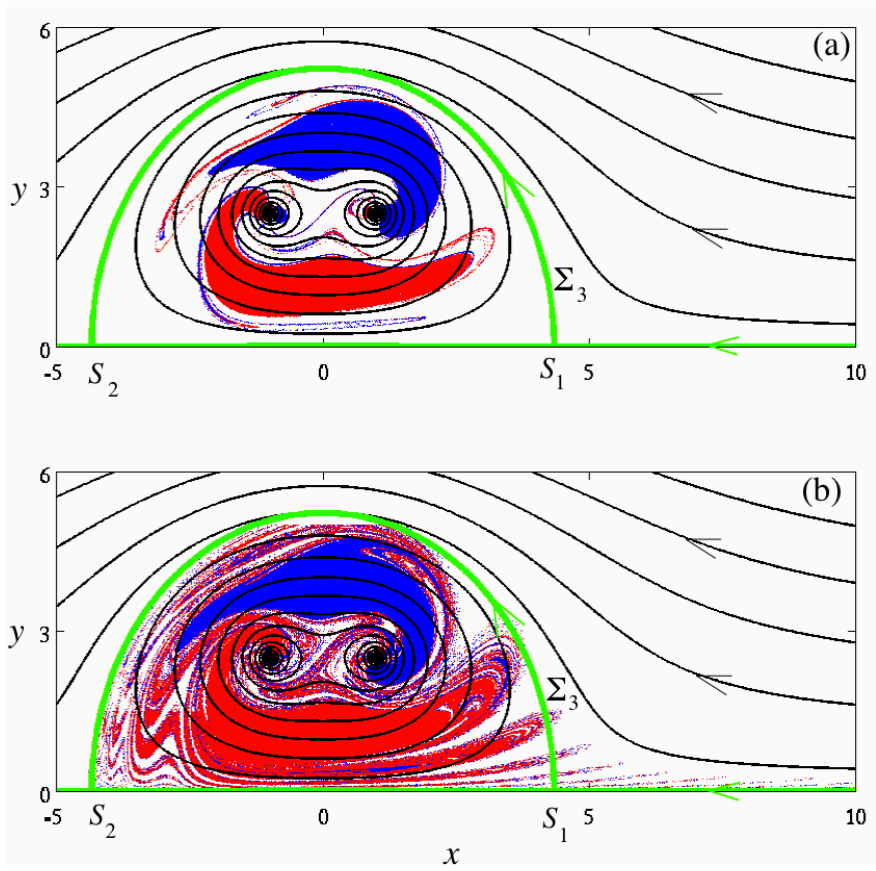


FIG. 10. Bounded versus unbounded basins of attraction. Red and blue represent the basins of attraction for (a) point P_1 and (b) point P_2 in the diagram of Fig. 9, obtained using simulations of the exact potential flow. The continuous lines represent instantaneous streamlines. In contrast with panel (a), the basins of attraction in panel (b) extend outside the external separatrix Σ_3 , demonstrating the existence of trapping from the open flow.

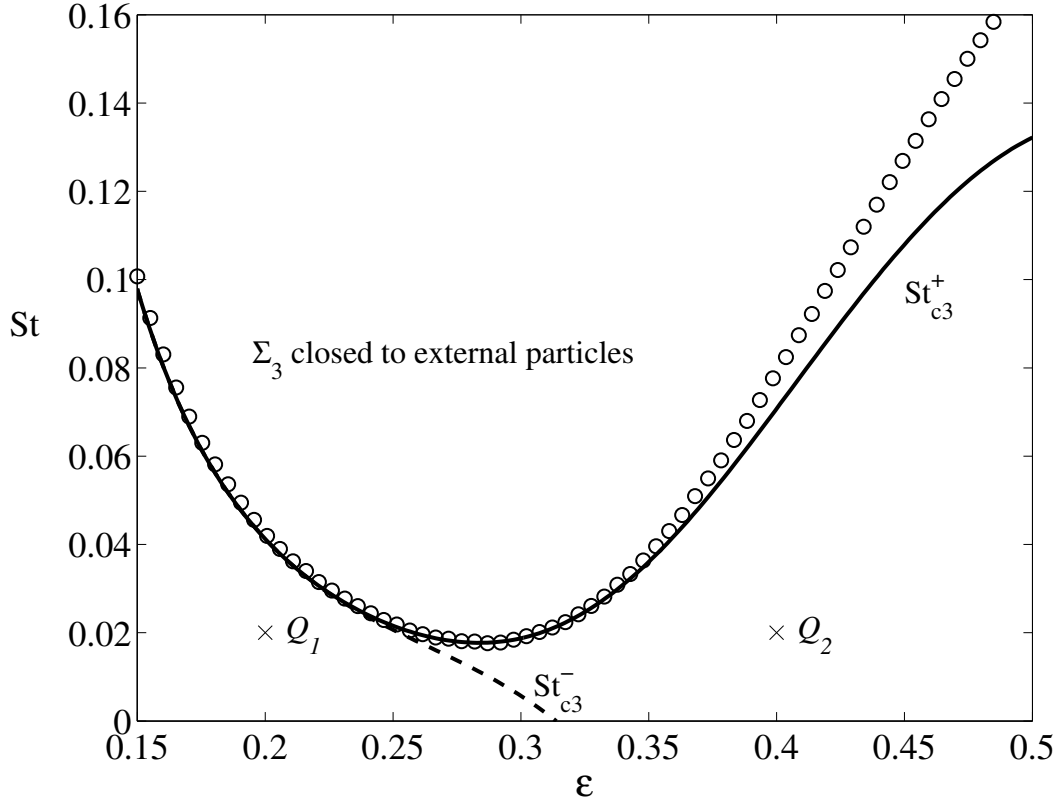


FIG. 11. Trapping diagram for heavy particles in the presence of gravity for a horizontal wall. The solid and dashed curves correspond to the theoretical critical Stokes numbers $St_{c_3}^+$ (Eq. (33)) and $St_{c_3}^-$ (Eq. (34)), respectively. These curves separate three possible behaviors determined by the Melnikov function associated with Σ_3 , in which particles can spiral out ($St > St_{c_3}^+$), spiral in (such as for point Q_1), or go both in and out (such as for point Q_2) across this separatrix. Circles correspond to a numerical verification of $St_{c_3}^+$. The diagram was generated using the choice $V_T = 0.003$ for the non-dimensional settling velocity.

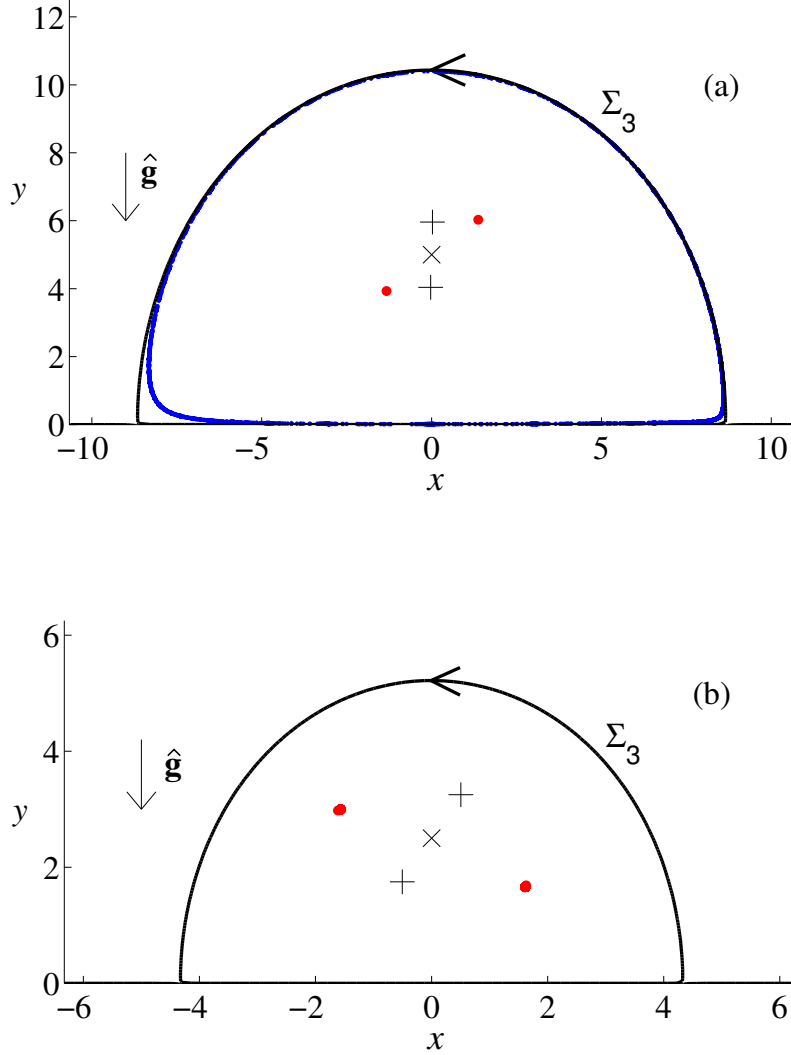


FIG. 12. Attractors in the presence of gravity for a horizontal wall. Colors indicate snapshots of the attracting sets for (a) point Q_1 and (b) point Q_2 in the diagram of Fig. 11, where the plus symbols indicate the vortices at the same instant. The attracting sets were traced by evolving for a long period of time particles released in the open flow near the wall and particles released in the closed flow covering the vortices. In case Q_1 , particles from the open flow cross the separatrix Σ_3 under the sole effect of gravity and converge toward a limit cycle (blue) right inside the separatrix; such particles cannot reach the point attractors (red) in the neighborhood of the vortices. Particles released inside the closed component of the flow can either converge to the limit cycle or be captured by the point attractors. In case Q_2 , a heteroclinic tangle exists near Σ_3 and there is no limit cycle. The point attractors (red) can now trap not only particles from the closed flow but also a fraction of the particles from the open flow. The simulations were performed using the exact potential flow.

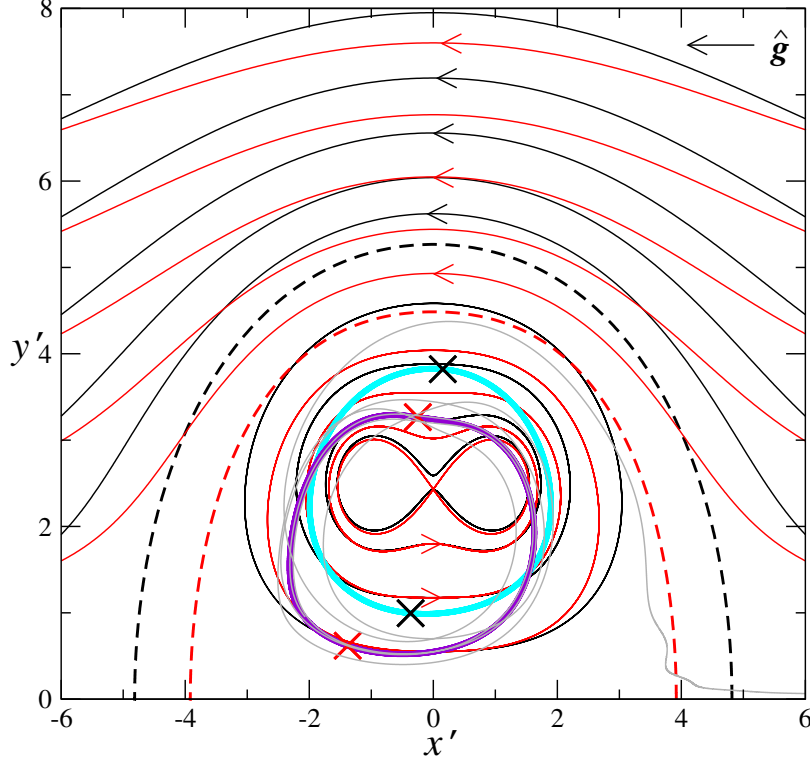


FIG. 13. Particle trapping in the presence of gravity for a vertical wall. Snapshot of the streamlines of both the fluid flow (continuous black lines) and the effective (“particle”) streamfunction corresponding to the leading-order velocity field of heavy particles under gravity (continuous red lines). Also shown are the corresponding instantaneous separatrices (dashed lines) and the attracting points in the absence (black cross symbols) and presence (red cross symbols) of gravity at the same instant. The projections of the orbits of the attracting points into the physical space are represented in cyan and violet, respectively. The grey line shows the trajectory of a representative particle from the open flow captured by a point attractor. In these simulations we used $\varepsilon = 0.4$, $St = 0.006$, and (for the presence of gravity) $V_T = 0.28$. The trapping of heavy particles from the open flow is observed under these conditions, and thus persists even in the presence of a strong gravitational field along the average direction of the fluid (in the reference frame of the center of vorticity).

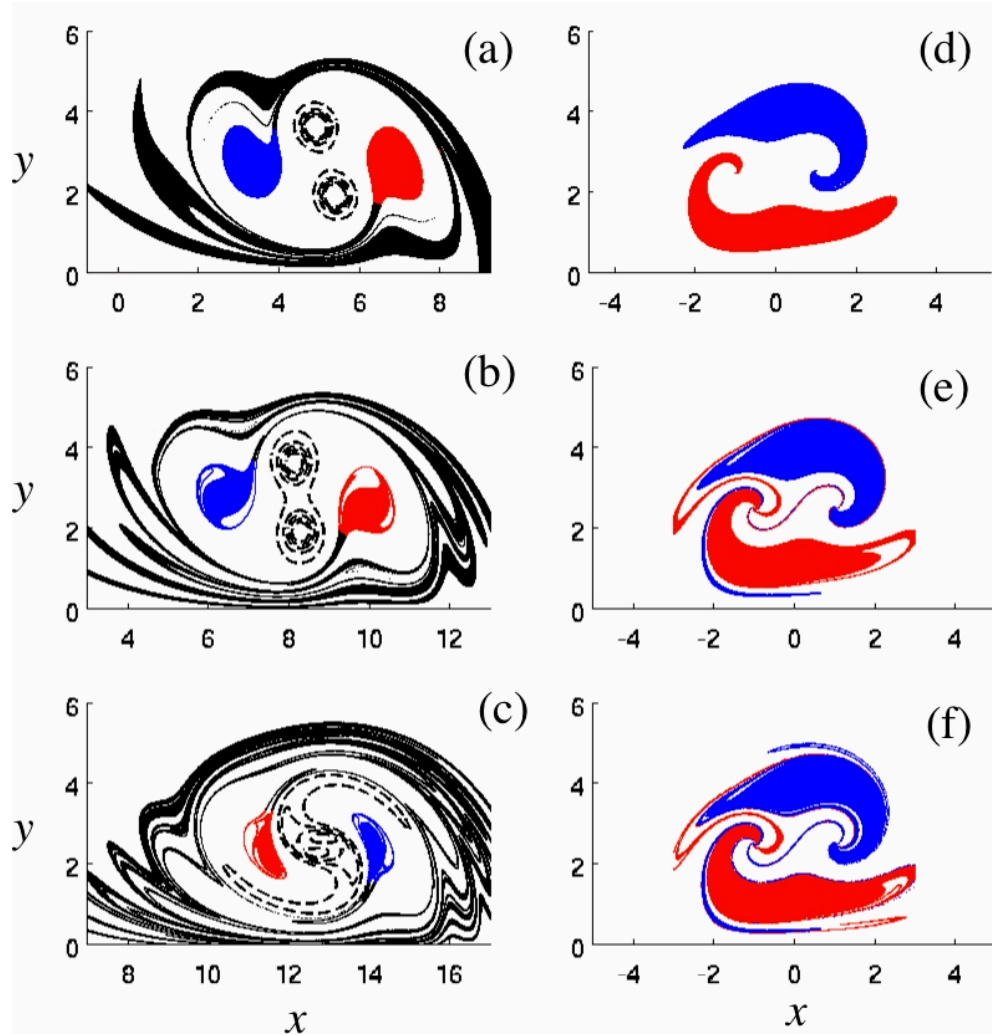


FIG. 14. Fractal-like basin boundaries in Navier-Stokes simulations. (a-c) Starting with heavy particles uniformly distributed in a region that includes the vortices at $t = 0$, the panels show the position of the particles at times $t = 7.1$ (a), 12.4 (b) and 19.4 (c). For the purpose of this illustration, particles marked with blue and red are considered trapped by the corresponding attractors, and dashed lines are iso-vorticity contours indicating the position of the vortices (same iso-values in all panels). (d-f) Initial positions of the trapped particles of corresponding colors in panels (a), (b), and (c), respectively. The symmetry line is located at $y = 0$ and only the top two vortices are shown. The flow Reynolds number Re is equal to 400. The other parameters are $St = 0.07$ and $\varepsilon = 0.4$. Note that the set defined by the initial conditions of the trapped particles becomes filamented as time increases.

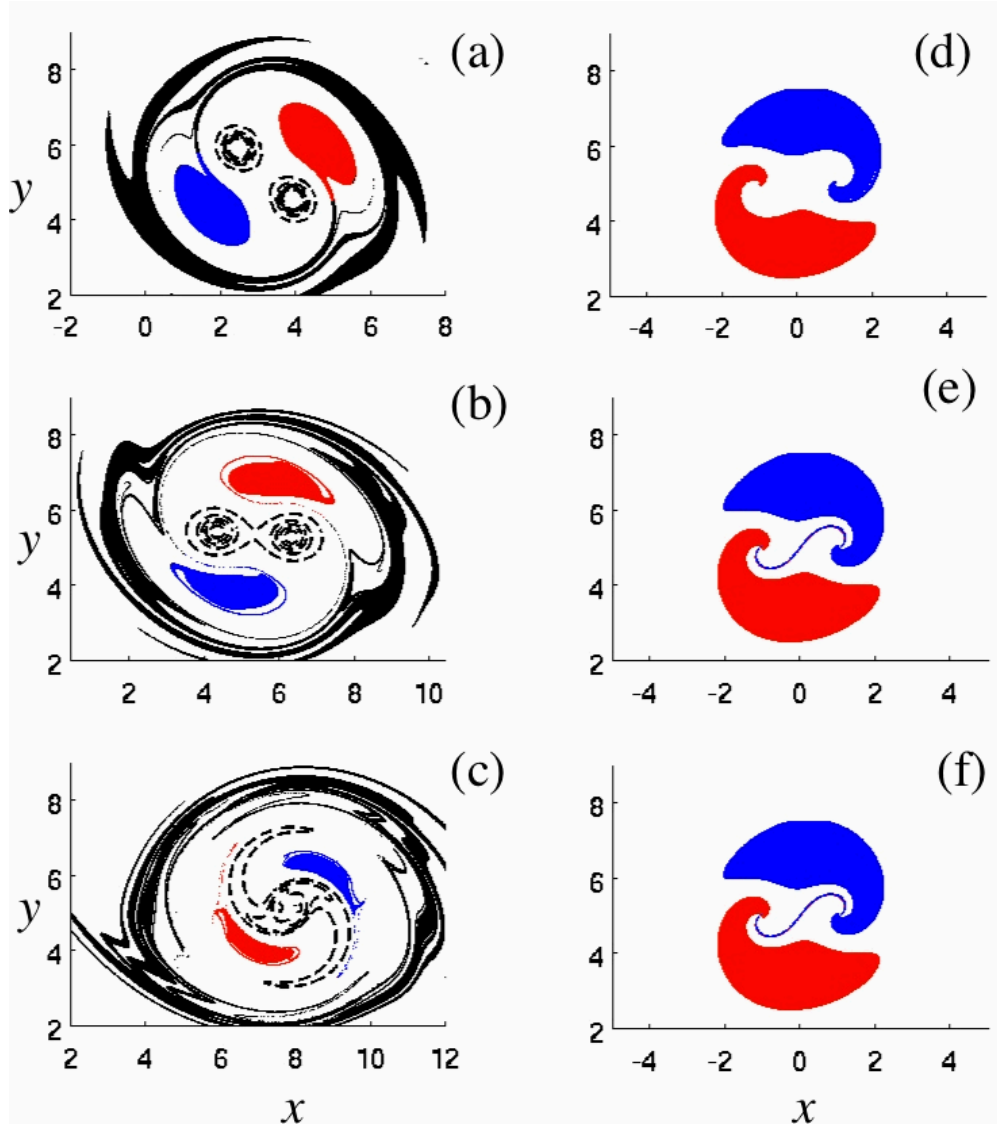


FIG. 15. Counterpart of Fig. 14 for smooth basin boundaries. Here, St and Re are the same as in Fig. 14 and $\varepsilon = 0.2$, which is above the critical distance to the symmetry line for the basin boundaries of the corresponding potential flow to become smooth. The particle distributions in panels (a-c) are represented at times $t = 8.3$ (a), 14.9 (b), and 22.0 (c). The corresponding colored regions in panels (d-f) defined by the initial positions of the particles trapped remain non-filamented as time increases, which further illustrates the agreement between potential flow predictions and Navier-Stokes simulations.

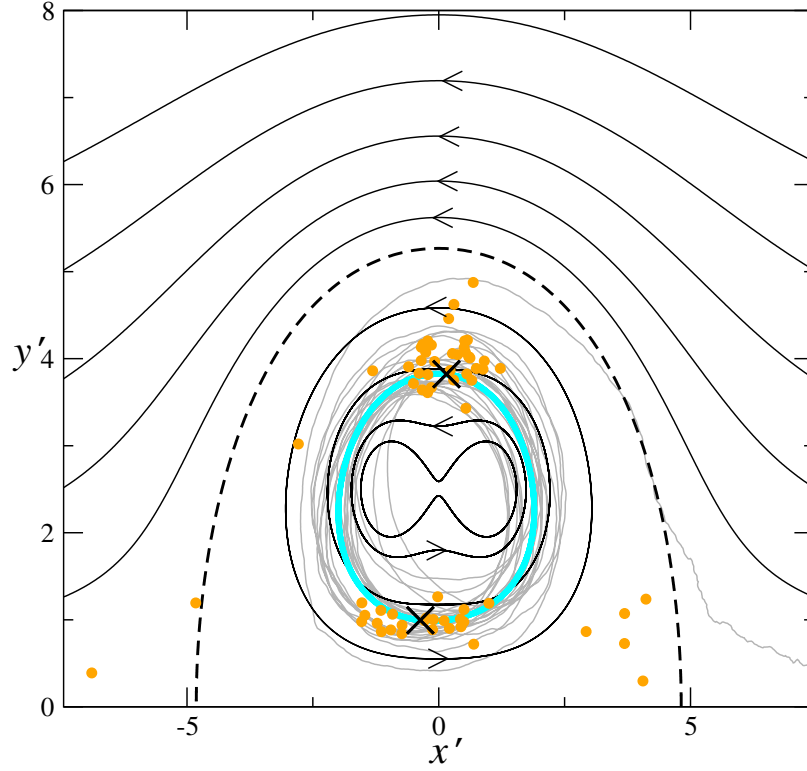


FIG. 16. Particle trapping in the presence of noise. Heavy particles released in the open flow and subject to noise are shown after 30.25 times the period of the fluid (orange dots) along with the projection of the full trajectory of one such particle (grey line). The attracting points of the deterministic dynamics at the same instant are marked with cross symbols and their orbit is shown in cyan. Also shown are the instantaneous streamlines (continuous back lines) and external separatrix (dashed black line) of the deterministic flow dynamics. The parameters are $\varepsilon = 0.4$, $St = 0.006$, and (for the presence of noise) $Pe = 600$.

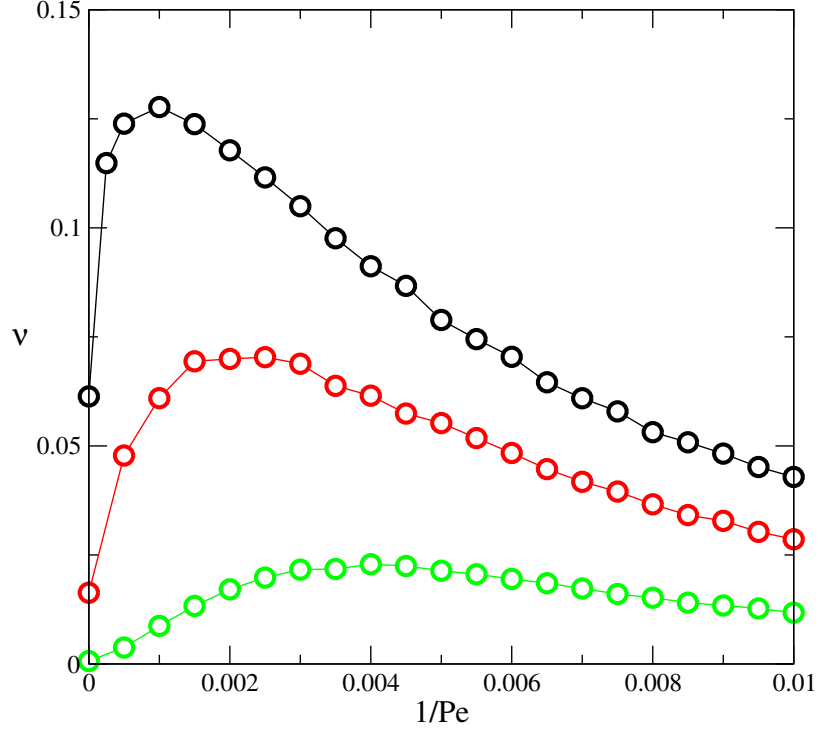


FIG. 17. Fraction ν of particles trapped as a function of the noise intensity $1/Pe$. The different curves correspond to $St = 0.005$ (black), 0.007 (red), and 0.010 (green), for $\varepsilon = 0.4$. Each data point corresponds to a total of 2×10^5 trajectories for particles released from a uniform distribution along the line segment $x = 5$ and $0 \leq y \leq 0.5$. As a criterion for trapping in the presence of noise, we regarded as trapped the particles that performed at least 40 revolutions around the corresponding attracting center.